INL/RPT-23-72642
Revision 0

Study of Storage Requirements and Costs for Shaping Renewables and Nuclear Energy

FY23 Summary Report

May | 2023

Paul Talbot
Aaron Epiney
Idaho National Laboratory

So-Bin Cho
Xiaodong Sun
Todd Allen
University of Michigan (UM)

IES
Integrated Energy Systems

INL/RPT-23-72642
Revision 0

Study of Storage Requirements and Costs for Shaping Renewables and Nuclear Energy

FY23 Summary Report

Paul Talbot
Aaron Epiney
Idaho National Laboratory
So-Bin Cho
Xiaodong Sun
Todd Allen
University of Michigan (UM)

May | 2023

Idaho National Laboratory
Idaho Falls, Idaho 83415

http://www.inl.gov

Prepared for the
U.S. Department of Energy
Office of Nuclear Energy
Under DOE Idaho Operations Office
Contract DE-AC07-05ID14517

Page intentionally left blank

ABSTRACT

To decarbonize electricity generation primarily by using wind and solar resources, it is likely that additional low (or zero) carbon dioxide (CO_2) alternatives will be required for ensuring a reliable electricity supply. This study extends the work and modeling framework that we consolidated in FY 2022, by assessing the zero-CO_2 pathways of a Texas power system in which the availability of variable renewable energy (VRE), nuclear energy, and energy storage types (i.e., battery and thermal energy storage [TES]) are considered the sole resources available for expansion.

Using the Risk Analysis Virtual Environment (RAVEN) and Holistic Energy Resource Optimization Network (HERON) frameworks, this study investigates the market of two nuclear energy technologies (i.e., large light-water reactors [LWRs] and LWR-type small modular reactors [SMRs]) under two plausible storage coupling scenarios (i.e., electric coupling and direct thermal coupling). We also explore optimal environments for nuclear energy deployment, and identify key performance characteristics that make nuclear energy economically viable in areas with significant intermittent energy sources.

Our analysis encompasses 24 cases. We model the least-cost grid systems, highlight the potential for a coupled LWR-TES approach, and utilize SMRs to achieve deep decarbonization in an affordable, technically feasible manner. We also examine seasonal variations in balancing electricity supply and demand, and account for varying performance, costs, and grid constraints. Overall, the findings of our modeling afford valuable insights for supporting future technology investment decisions in the energy sector.

Page intentionally left blank

CONTENTS

FIGURES

TABLES

Page intentionally left blank

ACRONYMS

ERCOT	Electric Reliability Council of Texas
HERON	Holistic Energy Resource Optimization Network
LDS	long-duration storage
LWR	light-water reactor
O&M	operations and maintenance
RAVEN	Risk Analysis Virtual Environment
SDS	short-duration energy storage
SMR	small modular reactor
SCOE	system average cost of electricity
TES	thermal energy storage
VARMA	vector autoregressive moving average
VRE	variable renewable energy

Page intentionally left blank

1. INTRODUCTION

The shift toward decarbonized energy systems will increase the amount of electricity production from variable renewable energy (VRE) sources such as wind and solar. This creates a need for complementary clean backup generation assets, despite the economic challenges they present for nuclear developers, due to lower utilization rates. [1] Although recent long-term energy system modeling studies forecast increasing affordability of VRE and storage technologies, the role of existing and new nuclear energy technologies, [2] particularly advanced nuclear technologies, in future U.S. power markets is still widely debated due to the cost overruns and delays incurred by prior large nuclear projects. [3] Hence, it is crucial to (1) assess the competitiveness of nuclear energy across different cost structures and technologies under a wide range of technological and economic assumptions, and (2) identify optimal locations for nuclear energy deployment, as well as the performance characteristics that make nuclear energy economically viable in areas with significant additions of VRE.

To this end, we selected large light-water reactors (LWRs) and LWR-type small modular reactors (SMRs) as surrogates for existing nuclear plants and advanced nuclear technologies, respectively, as there are various commercially available or in-development nuclear technologies that feature different configurations in terms of core size, lifetime, and other operating parameters. Our analysis focuses on the zero-carbon-dioxide (CO_2) pathways of a Texas power system in which VRE, LWR, SMR, and two types of energy storage (i.e., battery and thermal) are considered the only resources available for expansion. While hybrid operation of nuclear energy to enable hydrogen production and desalination could provide cost-cutting opportunities for nuclear energy and energy storage technologies, our study focuses solely on future opportunities for nuclear energy within the electricity sector—excluding any cross-sector applications or interactions of electricity and heat (e.g., substituting zero-CO_2 electricity for fossil-fueled processes in industry and transportation)—and the resulting long-term growth in electricity demand. [4]

Thus, we aim to provide decision makers with insights into the optimal deployments of nuclear energy and energy storage technologies, and how their attributes (e.g., cost projections, flexibility, and level of inter-regional transmission capacity) affect these deployments in terms of the evolving energy landscape. By employing internally consistent simulation settings, we describe the key design space of nuclear energy and energy storage technologies, thus enabling informed technology investment decisions.

2. METHODS DESCRIPTION

2.1 Simulation Overview

We utilized the Risk Analysis Virtual Environment (RAVEN) and Holistic Energy Resource Optimization Network (HERON) frameworks to conduct a comprehensive case study for an Electric Reliability Council of Texas (ERCOT)-like system. The RAVEN framework accounts for various factors such as user-provided electricity demand time series, VRE generation profiles, cost assumptions, and technological constraints, and converts them into a mixed-integer linear programming problem. It then performs stochastic techno-economic analyses of predefined scenarios in order to minimize total system costs. [5] Each optimal electricity generation mix is characterized by either the net present value or system average cost of electricity (SCOE). Table 1 summarizes the inputs required, and the resulting vector autoregressive moving average (VARMA) outputs used, to create the synthetic data.

Table 1. RAVEN synthetic data creation inputs/outputs.

Key inputs	Key outputs
• 2018 Texas solar hourly profile • 2018 ERCOT wind hourly profile • 2018 ERCOT hourly demand • Cluster number • Identified seasonality based on FFT[a] • ARMA(p,q)[b]	• Clustered solar/wind hourly capacity factor and demand profile

[a] *FFT = fast Fourier transform*

[b] *ARMA, generally expressed ARMA(p,q), can be either an autoregressive or moving-average process, where p is the order of the autoregressive model (or number of lags) and q is the order of the moving-average process.*

To generate the data necessary for our study, we obtained the 2018 load data from ERCOT, along with the corresponding meteorological data from NASA. The weather data were then converted into an hourly wind capacity factor based on location and technology. [4],[6] This approach offers advantages over utilizing actual VRE generation profiles from ERCOT, since those datasets may not always reflect the true VRE potential in Texas, owing to maintenance or unexpected events. As illustrated in Figure 1 and Figure 2, we chose the 60th and 90th percentiles of the state's wind and solar generation profiles in order to align our data selection with the current trend in wind and solar deployment in Texas. It is worth noting that solar plants are predominantly located in populated cities, whereas wind power is relatively more evenly distributed across the state. Expanding the area for the generation profiles marginally decreased the capacity factor in comparison to cases in the top 10 percentile. Specifically, we saw the capacity factor decrease from 0.356 to 0.319 for wind, and from 0.201 to 0.184 for solar. The impact of these decreases on the optimal sizing of least-cost portfolios was insignificant, primarily due to our cost assumptions for the generation assets (see Table 4).

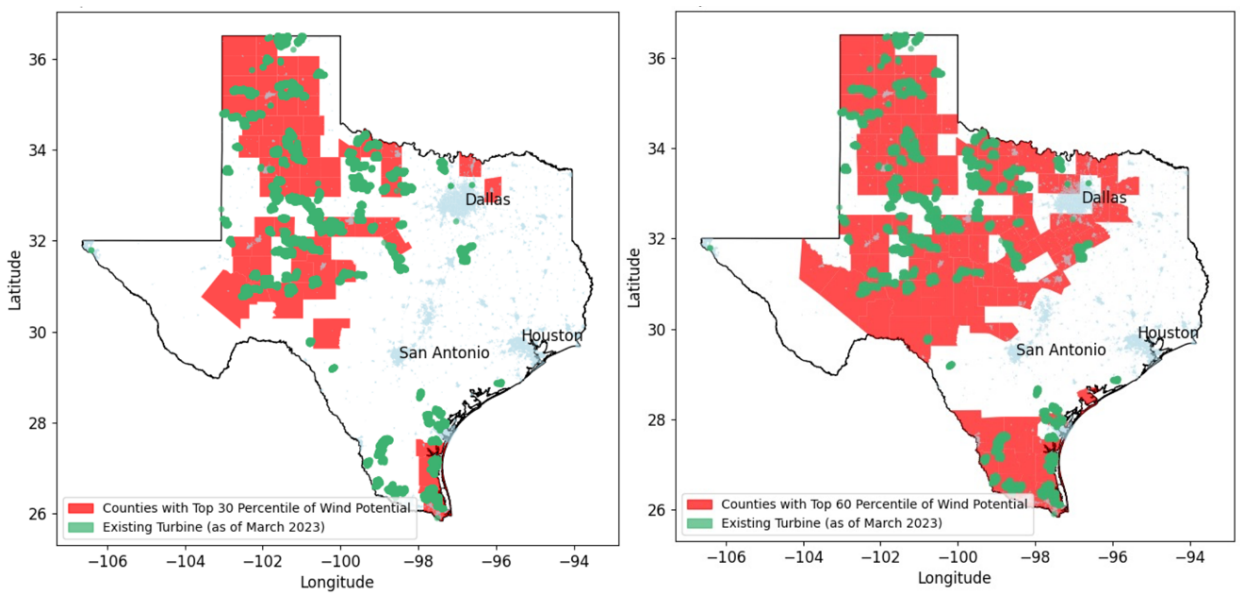

Figure 1. Comparison of wind generation estimates in selected areas: counties in the top 30th percentile (Left) and top 60th percentile* (Right) (* = selected percentile for study).

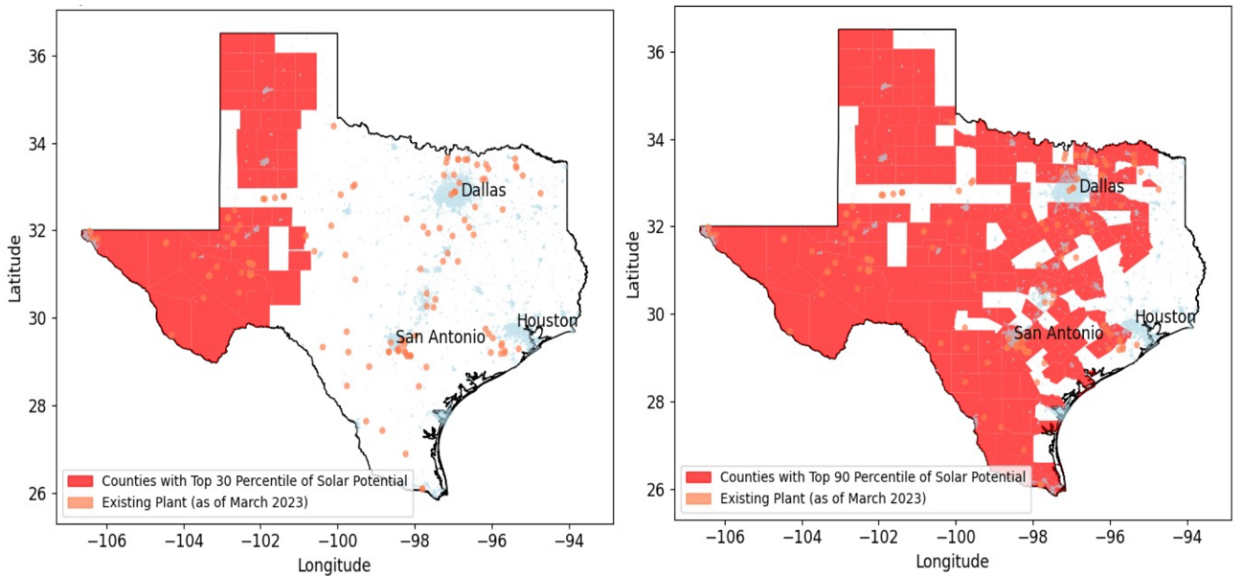

Figure 2. Comparison of solar generation estimates in selected areas: counties in the top 30th percentile (Left) and top 90th percentile* (Right) (* = selected percentile for study).

To simplify the modeling process, we utilized the VARMA algorithm in RAVEN to train and create synthetic load and VRE profiles. [7] The VARMA process identified statistical features of the original historical data and grouped them into three clusters, representing peak-summer, peak-winter, and off-peak periods. To ensure the validity of our VARMA model, which only applies to stationary time series, we performed Fourier detrending on load, wind, and solar profiles to remove seasonality. A time series is considered stationary if its probability density function—or joint probability density function, for VARMA—remains constant over time, without periodic patterns (e.g., daily, weekly, and seasonal electricity consumption/generation patterns). Figure 3 illustrates the amplitudes of significant periodicities identified by the fast Fourier transform, along with a set of periods representing strong cyclical behaviors

that occur hourly, mid-day (4 and 12 hours), daily (24 hours), weekly (120 and 168 hours), and monthly. Because Texas has relatively steady wind potential throughout the year, cyclic patterns in the wind data are less significant than those in load and solar potential data.

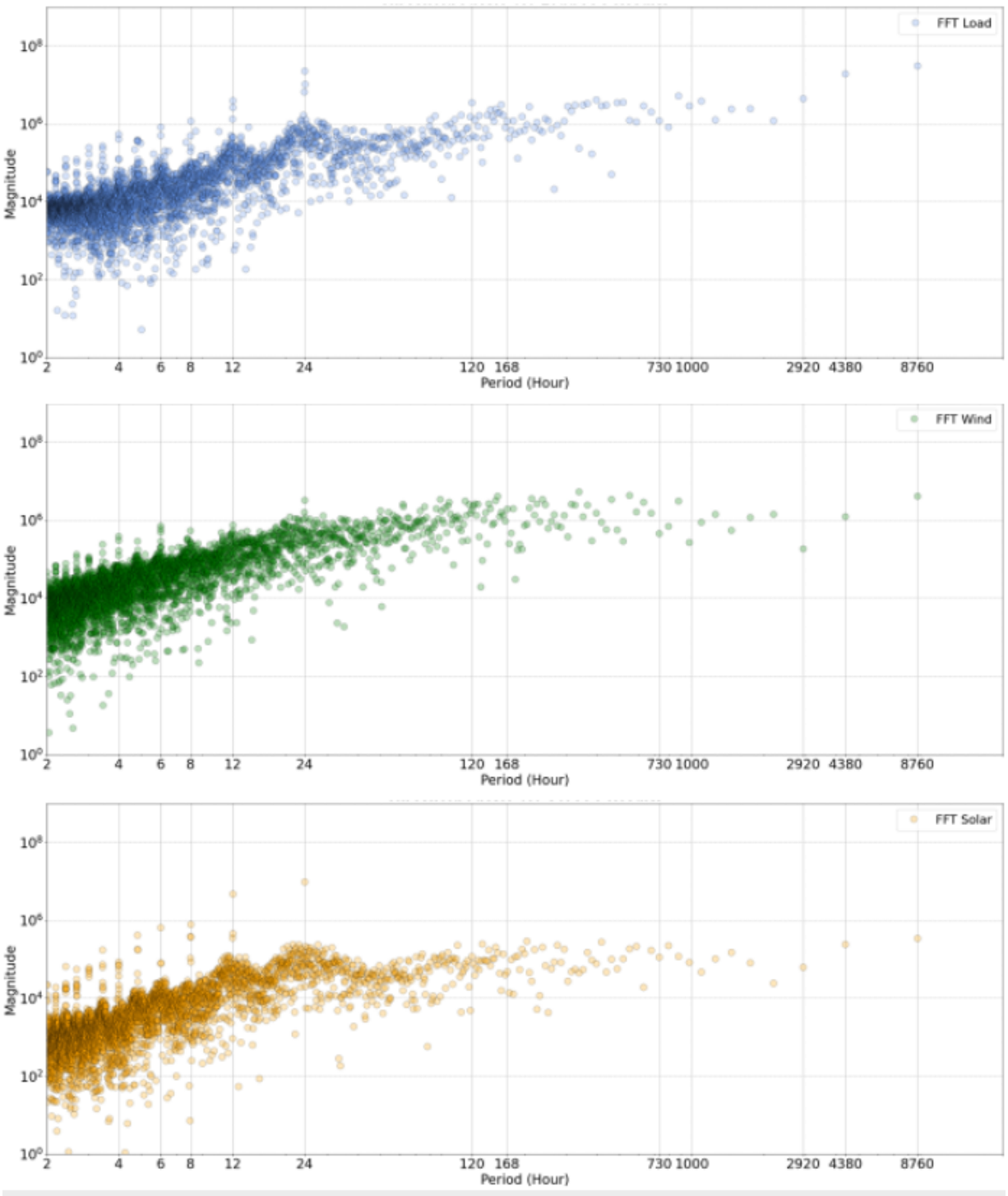

Figure 3. Fast Fourier Transform results for the 2018 ERCOT load data (top) and the 2018 Texas wind (middle) and solar potential data (bottom).

Table 2. HERON model inputs/outputs.

Key inputs	Key outputs

• Clustered solar/wind hourly capacity factor and demand profile
• Annualized capital costs, fixed operation and maintenance (O&M) costs, and variable O&M costs for each technology
• Operational parameters:
  o Storage duration
  o Heat-to-electric conversion efficiency
  o Ramp-rate
  o Minimum generation level
• Optimization variable resolution (see Table 3 for further details)
	• Optimized generation mix
	• Total system cost (net present value)
	• Hourly dispatch profile of each technology

Table 3. Optimization variable resolution for the analysis.

Variable	Range [increment]
Wind	60–230 GW [60:2:90, 94:4:230][a]
Solar	18–38 GW [18:2:38]
LWR	21–31 GW [21:1:31] 63.63–93.93 GWt [63.63:3.03:93.93] for thermal coupling[b]
SMR	1–10 GW [1:1:10] 3.03–30.3 GWt [3.03:3.03:30.3] for thermal coupling
Battery	10–50 GWh [10:2:50]
Thermal storage	3.03–30.3 GWt [3.03:3.03:30.3] for thermal coupling

[a] *In the interest of computational tractability, the ranges of technology capacities being employed in seeking least-cost portfolios were limited. For example, in each simulation the wind ranged from 60 to 90 GW, in relatively small increments of 2 GW and the range spanned from 94–230 GW with 4 GW increments.*

[b] *The increments were synchronized based on GW(e) scale in order to easily track the marginal effect of thermal storage or thermally coupled LWR and SMR units. For example, under the assumed thermal-to-electric conversion efficiency of 33%, the range of 63.63–93.93 GWt translates to a range of 21–31 GW(e).*

The ERCOT grid operates as a system that is largely independent of neighboring power networks, with limited interconnectivity. Thus, we determined the most cost-effective mix of generation and storage capacities to match the variable patterns in VRE generation and electricity demand throughout the year. This resulted in portfolios that reflect a grid sensitive to weather-related fluctuations in supply and demand. We then evaluated the system costs and optimal mixes under two different scenarios: an isolated grid and an interconnected grid featuring penalties for transferring excess or insufficient electricity to external grids. These tests allowed us to assess, in the context of regional coordination complexity, the value of nuclear energy as opposed to nuclear energy coupled with thermal energy storage (TES). To streamline the stochastic optimization workflow in RAVEN, we employed HERON, which combines the capacity and dispatch optimization steps. Capacity optimization identifies combinations of component capacities that are then held constant in the dispatch optimization. The dispatch optimization seeks the cost-minimizing portfolio that satisfies the synthetic load and wind profiles obtained via the VARMA process, while also accounting for the economic parameters and operational limits of each technology involved, as well as the grid interconnection constraint (see Table 2).

2.2 Modeling Assumptions and Scenarios

We obtained the cost parameters for each generation technology and annualized the overnight capital costs by using an 8% discount rate and the expected lifespan of each technology. [8],[9],[10] Two generic technologies (i.e., battery and thermal storage) were selected in evaluating the distinct functional roles of energy short-duration storage (SDS) and long-duration storage (LDS) technologies. Table 4 and Table 5 summarize the cost parameters for all the generating technologies considered in our study. The experimental design was comprised of 24 cases resulting from five possible scenarios: electrical coupling, nuclear-TES coupling, varying thermal storage, SMR cost projections, and thermal storage duration. In Table 6, these scenarios are denoted as Base, Thermal, Low-Thermal, Low-SMR, and Duration-Thermal, respectively. Our analysis accounted for the different grid interconnection sensitivities to system costs and optimal mixes by considering two distinct grid interconnections: an isolated grid (Cases 1–12) and an interconnected grid (Cases 13–24).

Table 4. Economic and technical characteristics of selected technologies (c: conservative, m: mid, l: low).

Technology	Capital Cost [$/kW][a]	Fixed O&M[b] [$/kW-y]	Variable O&M [$/MWh]	Min. generation [%]	Ramp rate [%/min]
Wind	1,500[c]	43.56[d]	0[d]	0	—
Solar	1,000[c]	19.87[d]	0[d]	0	—
LWR[e]	4,654[f]	117.99[d]	2.32[d]	100	0
SMR[e]	6,974[g] (C) 5,108[g] (M) 4,654[f] (L)	98[g]	3.08[g]	20[g]	5[g]
Battery[h]	261[i]	37.11[d]	0[d,g]	0	—
Thermal storage[e,j]	134 (C)[k] 94 (L)[k]	0[k]	0[k]	0	—

a. [$/kWh] for storage
b. [$/kWh-y] for storage
c. From Ziegler et al. (2019) [11]
d. From ANL (2020) [12]
e. Thermal-to-electric conversion efficiency (%) is modeled as 33% efficient—that is, thermal storage is modeled to have its turbine-generator system separated from the reactor loop.
f. From MITei (2019) [13]
g. From Breakthrough Institute (2020) [14]
h. Battery storage is modeled as SDS (1 hour) with a 90% round-trip efficiency.
i. From Dowling et al. (2020) [10]
j. Thermal storage is modeled as LDS (10 hour) with a 60% round-trip efficiency
k. From MITei (2022) [15]

Table 5. Annualized capital cost of technologies used to calculate the SCOE.

Technology	Life [years]	Discount rate [%]	Capital recovery factor	Annualized capital cost [$/kW]
Wind	30	8	0.089	133
Solar	30	8	0.089	89
LWR	60	8	0.081	376
SMR	60	8	0.081	563(C) 413 (M) 376 (L)
Battery	10	8	0.149	39
Thermal storage	20	8	0.102	136(C) 96 (L)

Table 6. Modeled scenarios for different configurations and technological assumptions.

Configuration				Capital Cost	
Scenario	Case	Generation	Storage (Duration)	Thermal Storage	SMR
Base	1/13*	W, S	B(1)	—	—
	2/14*	W, S, LWR	B(1)	—	—
	3/15*	W, S, LWR, SMR	B(1)	—	C
Thermal	4/16*	W, S, LWR	B(1), T(10)	C	—
	5/17*	W, S, LWR, SMR	B(1), T(10)	C	C
Low-Thermal	6/18*	W, S, LWR	B(1), T(10)	M	—
	7/19*	W, S, LWR, SMR	B(1), T(10)	M	C
Low-SMR	8/20*	W, S, LWR, SMR	B(1)	—	M
	9/21*	W, S, LWR, SMR	B(1), T(10)	C	M
	10/22*	W, S, LWR, SMR	B(1), T(10)	C	L
Duration-Thermal	11/23*	W, S, LWR, SMR	B(1), T(5)	C	—
	12/24*	W, S, LWR, SMR	B(1), T(5)	—	—

W, wind; S, solar; B, battery; T, thermal storage
C, conservative; M, mid-range; L, low technology cost assumptions (see Table 4 and Table 5)
* Cases with an interconnected grid constraint

In an interconnected grid, transfer capacities enable the balancing of lacking or excess electricity, thus preventing situations in which even a few hours of unmet demand significantly impact the least-cost portfolios. [15],[16] The term “transfer capacity” refers to the avoided capacity investment that would have been necessary if the grid was isolated. Prior studies have used penalty costs to model and estimate unmet demand, accounting for the investment risks and economic losses resulting from electric service interruptions. [17]–[20] In previous studies, two types of monetary penalties were utilized to estimate unmet demand risks: a constant (or lump-sum) penalty cost [17],[18] and a penalty function that varies with the amount of unmet demand. [19],[20] Although both approaches aim to assess risk, the penalty function strategy is more adaptive to the level of unmet demand. Although these penalties may oversimplify the balancing mechanisms of inter-regional transmission expansion, their implementation is useful in helping grid planners conceptualize the required new generation or storage capacity needed in light of different grid system reliability objectives. [21]

In fact, these penalty functions can be interpreted as equivalent to the willingness to invest additional funds into generation and/or storage capacity so as to prevent reliability disruptions. Therefore, we calculate the corresponding penalty costs per unmet demand by utilizing the National Renewable Energy Laboratory's simplified levelized cost of electricity equation, which considers the varying capacity factors of generation assets (see Table 7). [22] The penalty functions implemented in our study reflect the probabilities of unmet demand events in relation to the number of hours in a year. In situations involving infrequent disruptions, such as those triggered by extreme weather conditions, the capacity factor of supplementary generation assets could decrease, thereby increasing the penalties for unmet demand. Following a particular blackout in 2022, ERCOT reduced its cap from $9,000 to $5,000 per MWh, which is now the cap level for the spot market price of electricity. To account for this, we use an exponential penalty function with a $5,000/MWh cap, as depicted in Figure 4. In HERON's transfer function module, the penalty to be paid is computed by multiplying the penalty function by the amount of unmet electricity for each hour.

Table 7. Penalty costs of unmet demand with respect to the capacity factor (which is expressed in terms of the total unmet demand hours as fraction out of a year).

	Penalty Cost for Two Possible Backup Solutions for External Grid Access [$/MWh]	
Total Unmet Demand Hours as a Fraction of the Number of Hours in a Year	Natural Gas Combined Cycle	Storage (Generic)
0.00137 (12 h / 8760 h)	6,841	10,988
0.00194 (17 h / 8760 h)	4,889	7,849
0.00274 (24 h / 8760 h)	3424	5,494
0.02740 (240 h / 8760 h)	343	549
The cost parameters used for the simplified levelized cost of electricity calculation are from [12].		

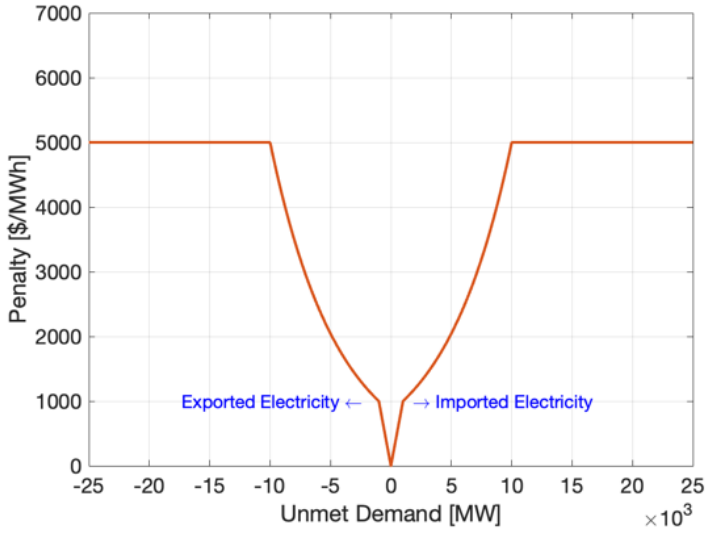

Figure 4. Implemented penalty function for unmet load.

Furthermore, our simulation relies on several simplifying assumptions. First, we assume a zero-carbon electricity sector (i.e., 0 g CO_2/kWh emission constraint), disregarding existing fossil fuel generating plants in ERCOT and conducting greenfield analyses. Second, we assume perfect foresight and ignore any forecast error in terms of the load and VRE profiles. Third, we focus on six technologies: wind, solar, LWR, SMR, battery storage, and thermal storage, as aligns with our greenfield modeling assumption. Finally, we consider a best-case scenario by disregarding transmission costs and constraints that may vary across geographic regions. This approach allows for macro-scale energy modeling with an hourly resolution that meets the system load through a combination of different agglomerated sources.

3. MODELING RESULTS

3.1 Base Cases

Figure *5* presents the dispatch results of the least-cost systems, both with and without nuclear technologies (LWR and SMR), with each subplot representing a typical day (24 hours) throughout the year. The number of days that each cluster represents is indicated in the legend, summing up to a full 365-day year when weighted by the number of days in each cluster. Wind availability is determined by hourly capacity factor and realized by multiplying the nameplate capacity during optimization. The black lines represent the clustered demand curves (as do the grey areas below 0 GW by depicting the inverse of the demand). At each hour, charging of battery storage is balanced with generation from wind/nuclear plus discharging from battery storage. Appendix A (Figure A-1 through Figure A-24) gives the cost-minimizing dispatch results for all cases.

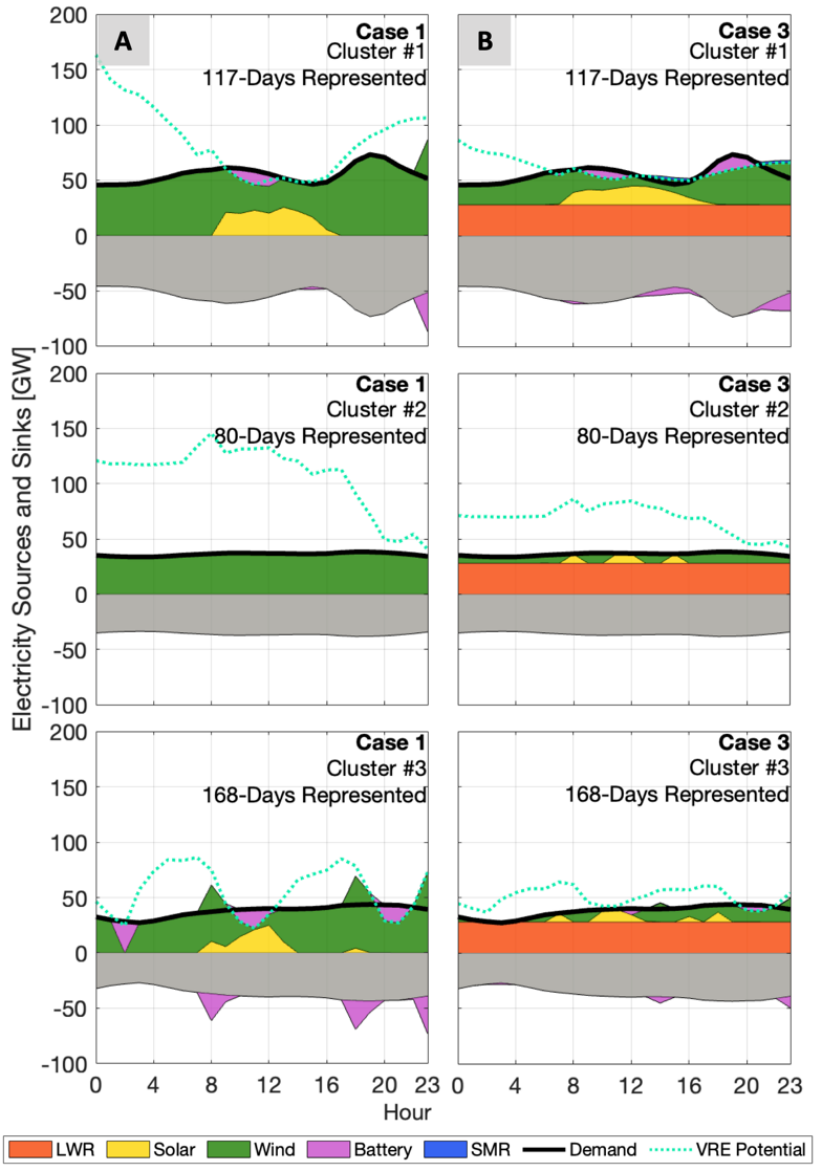

Figure 5. Example hourly operation of optimal generation capacity mix with a 1-day temporal extent.

This figure shows 1 day of stacked dispatch for each of three clusters under an isolated grid constraint, comparing the impacts of nuclear availability on system operation in Texas. (A) Case 1: no nuclear, (B) Case 3: LWR with conservative-cost SMR. In Case 3, the SMR dispatch is indiscernible from the figure, due to its minimal contribution of only 1.2% (i.e., 2 GW) to the least-cost portfolio (see Figure 6).

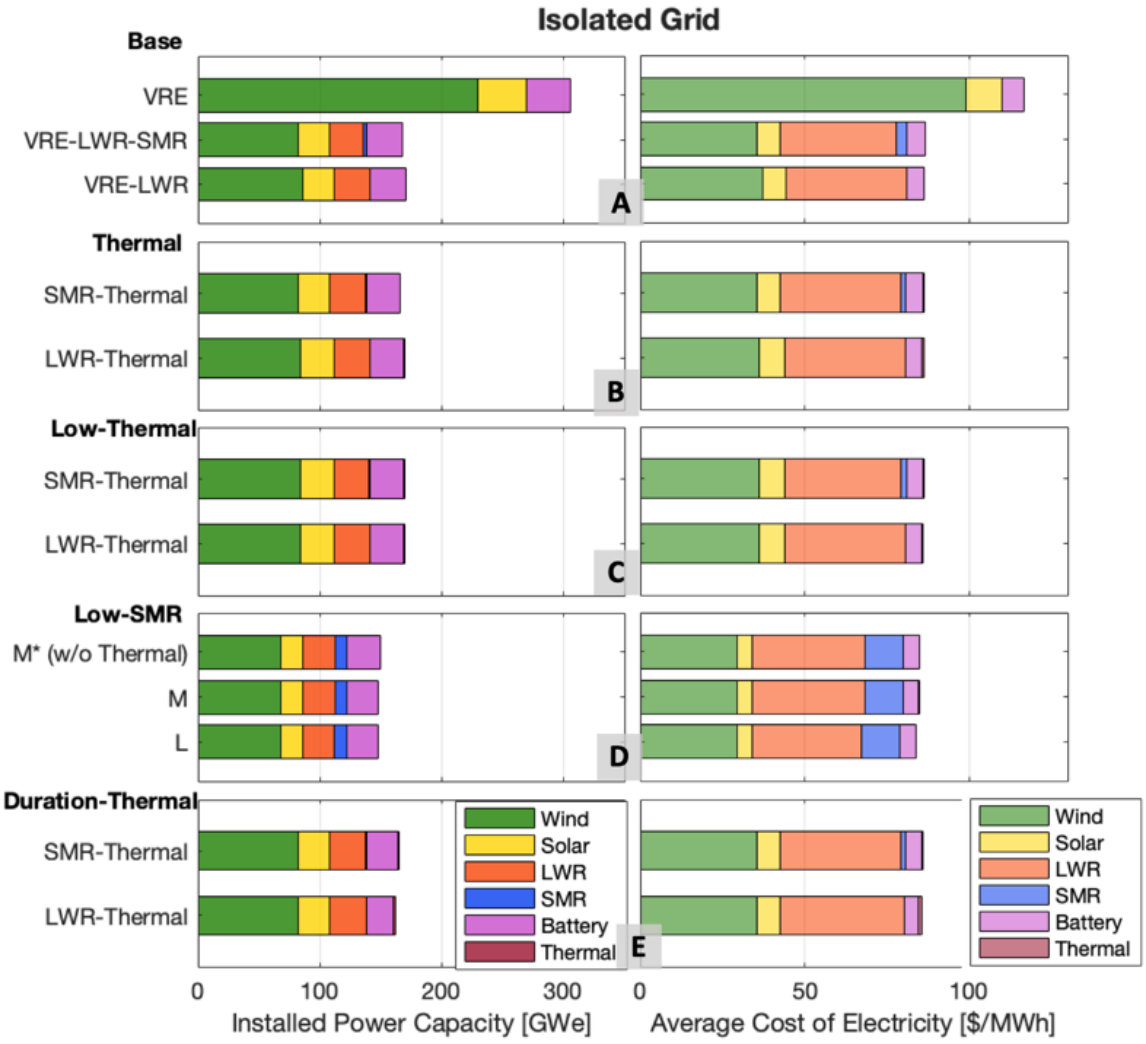

Figure 6. System impacts of (A) base scenarios, (B) nuclear-TES coupling, (C) low-cost thermal storage, (D) low- and mid-cost SMR and (E) reduced thermal storage duration on installed power capacity (left) and SCOE (right), in an isolated grid.

M, mid-range; L, very low technology cost levels (see Table 4).

**This analysis is limited to an electric-coupling-only grid system, as in the base cases (the top three bars). In this illustration, the battery is the sole energy storage technology deployed for optimization purposes.*

As shown in Figure *5*, electricity from battery storage is dispatched across the three clusters to shift wind generation and meet the morning peak demand (purple). A full year of chronological variability in both VRE generation and electricity demand was clustered based on their annual, weather-sensitive patterns. For instance, Cluster #3 (off-peak periods) in Figure *5*A suggests that relying heavily on VRE leads to significant use of batteries during off-peak periods, potentially degrading the batteries more quickly than would light cycling (Cluster #3 in Figure *5*B). [23],[24] Cluster #1 in Figure *5*A captures summer peak periods in Texas when the wind resources decrease. In this case, a substantial amount of wind is added to meet demand during low-resource periods and to sufficiently meet air conditioning needs during evening peak demand (between 5 and 8 PM). Due to such overbuilding, wind generation must be significantly curtailed when its availability exceeds demand during low-demand periods (after 8

PM), winter (Cluster #2), and off-peak periods (Cluster #3) (shown as the vacant area between the VRE potential and the wind profile curve).

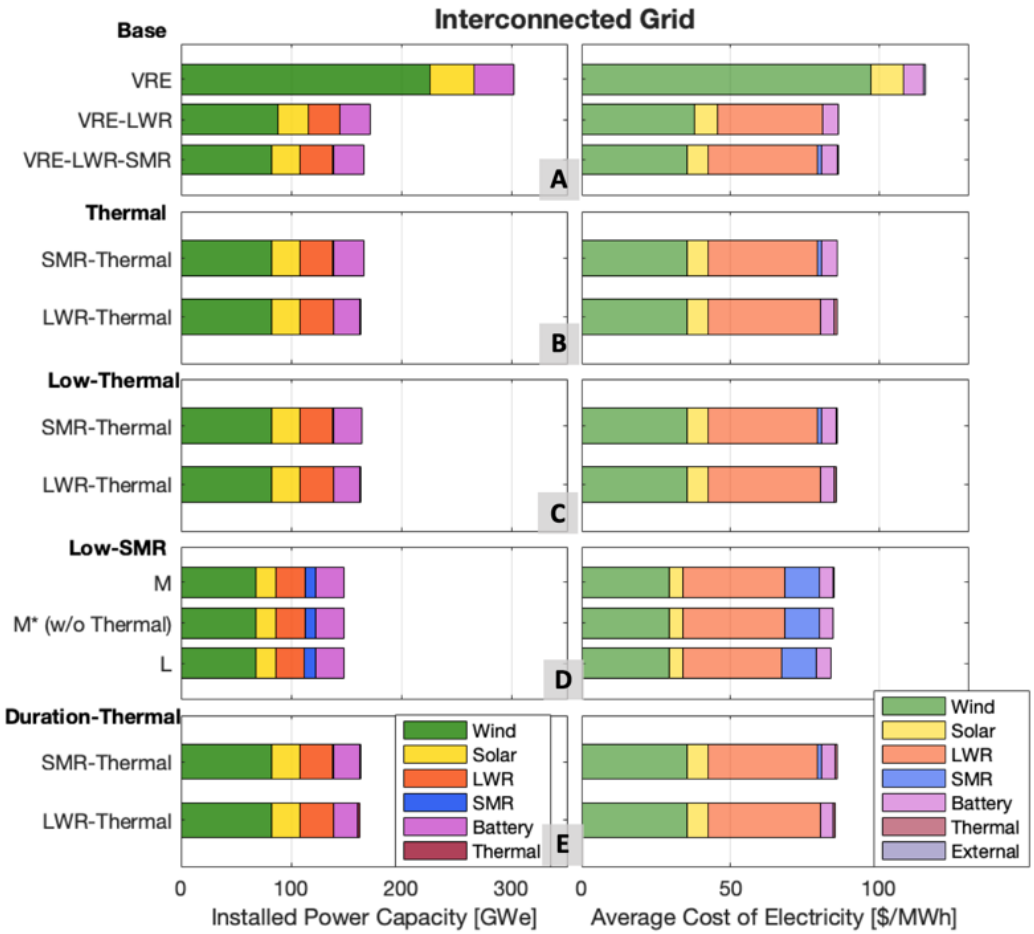

Figure 7. System impacts of (A) base scenarios, (B) nuclear-TES coupling, (C) low-cost thermal storage, (D) low- and mid-cost SMR, and (E) reduced thermal storage duration on installed power capacity (left) and SCOE (right), in an interconnected grid.

The least-cost capacity mixes and SCOE were analyzed for various cases in both an isolated and interconnected grid. Figure 6 and Figure 7 present the results in descending order of SCOE. It should be noted that SCOE includes annualized capital costs, fixed/variable O&M costs of generation and storage, and penalties for unmet demand (Figure 7). Figure 6A and Figure 7A illustrate that the presence of LWR technology mainly displaces wind capacity, even when dispatchable SMR is available (in the conservative cost projection). For cases in which the base scenarios involve VRE-only (Cases 1 and 13), a rapid increase in both installed power capacity and SCOE was observed in comparison to cases in which LWR (Cases 2 and 14) and LWR-SMR (Cases 3 and 15) technologies were available. When SMR was available as a dispatchable power generation technology in an interconnected grid, there was a slight reduction in SCOE relative to the VRE-LWR case (Case 14 vs. 15). However, adding SMR was slightly more expensive (0.4%) in an isolated grid (Case 2 vs. 3).

3.2 System Impacts of Grid Interconnection, with Monetary Penalty

Sepulveda et al. [25] pointed out that limited transmission capacity with no economic cost assigned for transfer capacity can significantly reduce system costs in comparison to system isolation. However,

one recent study [15] suggests that grid interconnection may not have a major impact on system costs and optimal capacities when a high penalty for transferring capacity ($50,000/MWh) is assumed. This penalty acts as an enforcement mechanism to incentivize including more generation/storage capacity to meet demand. Nonetheless, this approach does not fully address the economic balance mechanism of grid interconnection, which is sensitive to economic signals such as the probability or magnitude of unmet demand. To better represent potential behavioral changes caused by grid interconnection, we extended this analysis by factoring in differentiated costs for flexibility levels, following the methodology of Epiney et al. [20]

In our analysis, we found that, in the given scenarios, grid interconnection leads to a substantial decrease (-7% to -14%) in battery capacity, especially in the LWR-thermal scenarios (Cases 16 and 18), in which thermal storage is available and the cost of SMR is high (Table 8). Our reliability results, shown in Table 9, indicate that the reliance on grid interconnection increases sharply (by 22% and 78% for the number of unmet events and total unmet demand, respectively) as thermal storage replaces battery storage for long-term peak shaving (Case 14 vs. 16), whereas the reliance decreases (by 44% for total unmet demand) for the case with conservative-cost SMR (Case 15 vs. 17). This suggests grid interconnection to be a viable option for system decarbonization if the cost of unmet demand is comparable to other SDS options (e.g., battery), and that substitution effects are evident at a lower fraction of peaking generation (SMR).

Table 8. Effect of interconnection on optimal installed power capacities and energy capacities [%].

Scenario	Case	Wind	Solar	LWR	SMR	Battery	Thermal storage
Base (VRE)	1/13*	-2	0	—	—	0	—
Base (LWR)	2/14*	2	8	-3	—	-7	—
Base (SMR)	3/15*	0	0	4	-50	-7	—
Thermal (LWR)	4/16*	-2	-7	3	—	-14	100
Thermal (SMR)	5/17*	0	0	0	0	0	-67
Low-thermal (LWR)	6/18*	-2	-7	3	—	-14	100
Low-thermal (SMR)	7/19*	-2	-7	4	0	-7	0
Low-SMR (M*)	8/20*	0	0	0	0	-7	—
Low-SMR (M)	9/21*	0	0	0	0	0	0
Low-SMR (L)	10/22*	0	0	0	0	0	0
Duration-thermal (LWR)	11/23*	0	0	0	—	0	-10
Duration-thermal (SMR)	12/24*	0	0	0	0	-8	50

M mid-range; L, very low technology cost levels
M* This analysis is limited to an electric-coupling-only grid system
* Cases with an interconnected grid constraint

NOTE: *The effects of allowing the transfer of lacking or excess electricity are shown as the optimal (energy) capacity difference [%] between cases involving an isolated grid and cases involving an interconnected grid (see Figure 6 and Figure 7).*

Table 9. Interconnected case reliability results across different model configurations and cost levels.

Scenario	Case	No. of unmet events	Max. duration [hour]	Total unmet demand [GWh]	Unmet demand fraction [%]
Base (VRE)	13	168	1	201	5.34
Base (LWR)	14	234	1	51	1.37

Scenario	Case	No. of unmet events	Max. duration [hour]	Total unmet demand [GWh]	Unmet demand fraction [%]
Base (SMR)	15	117	1	107	2.84
Thermal (LWR)	16	285	1	91	2.41
Thermal (SMR)	17	117	1	60	1.60
Low-thermal (LWR)	18	285	1	91	2.41
Low-thermal (SMR)	19	234	2	95	2.53
Low-SMR (M*)	20	117	1	16	0.42
Low-SMR (M)	21	0	—	—	—
Low-SMR (L)	22	0	—	—	—
Duration-thermal (LWR)	23	285	1	49	1.31
Duration-thermal (SMR)	24	234	2	35	0.92

- *No. of unmet events: number of unmet events; Max. duration: maximum duration of a single unmet demand event; Unmet demand fraction: total unmet demand as a fraction of nominal load*
- *Unmet demand events are identified for each cluster over a 1-day optimization window and weighted by the number of days in each to represent a full year.*

For example, Table 8 shows that assuming a mid-cost SMR (without thermal storage) minimizes the interconnection usage (Case 20), and that reliance on grid interconnections is eliminated when thermal storage is coupled to a mid- or very-low-cost SMR. This in turn yields the same optimal mixes and system costs (Cases 21 and 22) in comparison to their own respective cases in isolation (Cases 9 and 10). Although SMR technology is still relatively expensive at the conservative cost projection for SMR (Case 15), such a reliable dispatchable resource is especially beneficial for preventing unmet demand events at a given power system level, compared to the VRE (Case 1) and the LWR scenarios (Cases 14, 16, 18, and 23). When both SMR and thermal storage are excluded (Case 14), greater interconnection usage (Table 9) and the resulting monetary penalty lower the optimal capacity of the LWR (Table 8). Although LWR deployment can noticeably reduce system costs and capacities in our modeling, such benefits would be more sensitive to regional interconnection than they would be in isolation. In this case, VRE capacities and grid interconnection serve as a direct substitution for LWR.

3.3 System Impacts of Coupling Nuclear Technology to Thermal Storage

Compared to batteries, thermal storage has the potential to be a cost-effective option for LDS, despite its relatively low round-trip efficiency (see Table 4). [10],[15],[17] In particular, TES could represent a valuable solution to the extended seasonal mismatch between VRE potential and demand—a mismatch that can persist for several months (see Figure 5A). Though previous studies have shown that coupling nuclear technology with TES can produce a more flexible and affordable asset in a fully decarbonized system, research on the potential of LDS to help enable deep decarbonization has been limited to intra-model comparisons of system costs, optimal capacities, etc. [10],[11],[15],[17],[25] To address this gap, we investigated the operational characteristics of nuclear-TES coupled systems and their impact on least-cost portfolios, under different thermal storage durations and cost projections for SMR and thermal storage (see Table 6).

In a recent study, three nuclear-TES coupling options were explored to minimize the dynamic impacts of thermal storage operation on the nuclear power plant (NPP): (1) standalone NPP-TES coupled with a secondary power generation cycle, (2) a directly coupled NPP-TES system, and (3) an integrated

NPP-TES coupled with an oversized primary turbine. [26] To investigate the interplay between thermal storage and base (LWRs) or peaking capacity (SMRs), we selected the first coupling option, in which a nuclear reactor and a thermal storage system have their own independent steam generators and associated auxiliary systems (e.g., piping). In this coupling geometry, during the charge cycle, steam is diverted from the primary turbine to a thermal storage system. During the discharge cycle, a secondary turbine is employed without interrupting the NPP operation. [26]

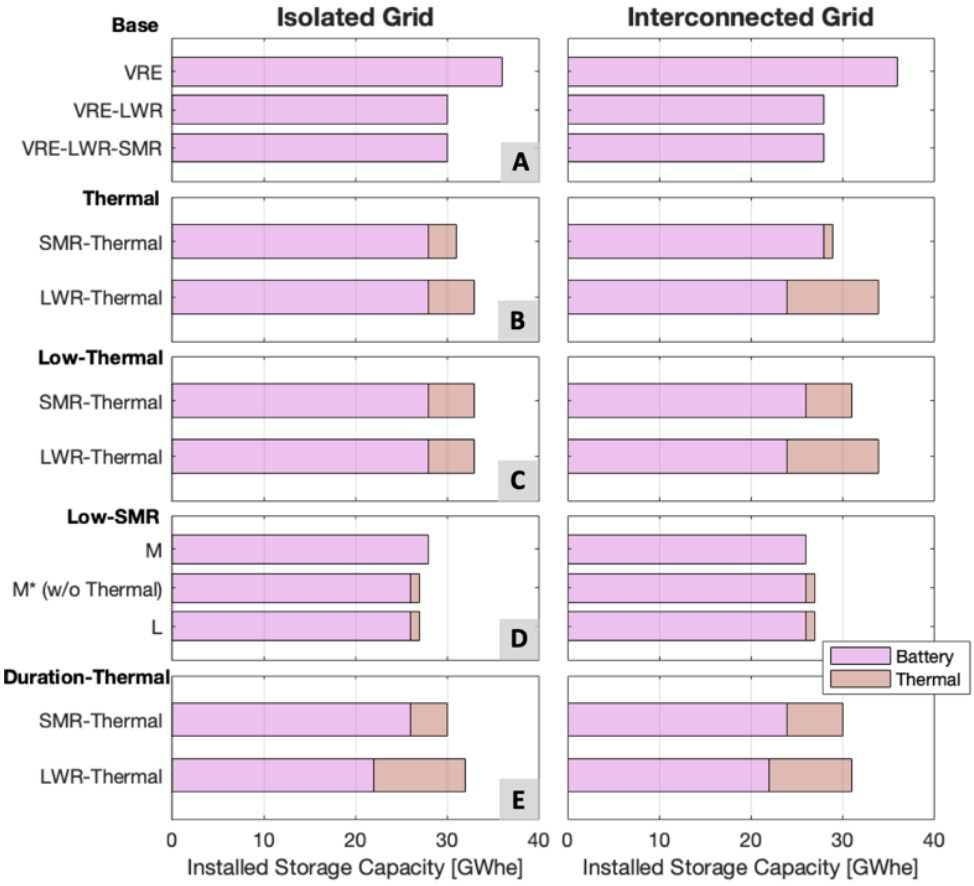

Figure 8. Comparison of installed storage capacity across scenarios, both with and without grid interconnection.

We examined how changes in coupled nuclear technologies, thermal storage costs, SMR costs, and thermal storage duration impacted the installed storage capacity of the least-cost system (Figure 8B–E). The results showed that, when coupled with an SMR, the installed thermal storage capacity becomes reduced or eliminated (Figure 8C and Figure 8D) because thermal storage systems with independent turbines compete with the SMR, decreasing the capacity of the relatively expensive resource and increasing the utilization of lower-cost resources in each scenario. For instance, in cases that assume an isolated grid, a 30% reduction in thermal storage costs would decrease the SMR capacity factor by 8% (Table 10). On the other hand, reducing SMR costs by 27% and 33% caused a significant thermal storage capacity decrease (up to 67%) in the isolated-grid cases, leading to a mix without thermal storage (Figure 8D). Similar tradeoffs between the SMR capacity factor and thermal storage capacity were observed in the interconnected grid cases, though the magnitude of the tradeoff can vary depending on the cost of unmet demand (Figure 4).

Table 10. Comparison of SMR capacity factors under different scenarios and grid constraints.

Scenario	Case	Capacity Factor		Capacity Sensitivity to Grid Interconnection [%]
		Iso.	Inter.	
Base (SMR)	3/15*	0.364	0.334	-7
Thermal (SMR)	5/17*	0.335	0.335	-7
Low-Thermal (SMR)	7/19*	0.309	0.321	-7
Low-SMR (M*)	8/20*	0.373	0.373	0
Low-SMR (M)	9/21*	0.378	0.373	0
Low-SMR (L)	10/22*	0.380	0.378	0
Duration-Thermal (SMR)	12/24*	0.339	0.361	-8

* Iso.: isolated grid; Inter.: interconnected grid.

NOTE: *The effects of allowing the transfer of lacking or excess electricity are shown as the difference [%] between cases with an isolated grid and cases with an interconnected grid (see Figure 6 and Figure 7).*

In contrast, the cost of thermal storage did not significantly impact the deployment of LWR with thermal storage in either isolated and interconnected grids (Figure 8B and C). This suggests deployment of thermal storage to be more influenced by the availability of dispatchable capacities in each scenario than by cost considerations. Therefore, for SMR-TES coupling, thermal storage would compete with the SMR or other low-cost dispatchable resource options. Furthermore, the study revealed that, in an interconnected grid configuration, the additional flexibility enabled by LWR-thermal coupling facilitates a slightly deeper penetration of LWR, while the optimal sizing of the LWR remains the same (Figure 6A and B, Figure 7A and B; Table 8). These findings support prior research on the benefits of LWR, as it is a robust and predictable energy source across different integration approaches, with or without thermal storage [13],[25].

We also investigated the impact of thermal storage duration on nuclear-TES coupling, while maintaining its capital cost of $134/kWh (see Table 11). Our findings indicate that deployment of thermal storage can further reduce the need for batteries, except for in the LWR-thermal coupling scenario involving a grid interconnection. This suggests that, in certain scenarios, thermal storage with reduced duration is better suited for SDS applications that compete against similar SDS options (battery and external grid). Figure 9 supports this claim by illustrating the amplitude of charge/discharge operations for the LWR-thermal scenario featuring an isolated-grid constraint (Case 4 vs. 11). The overlap between battery storage and thermal storage is also represented in Figure 6 as a mix of the light- and dark-pink colors in the darker shaded area. As the duration of thermal storage is reduced, its distribution becomes less diversified, while increasing the level of overlap at a depth of around -50–50%. Note that the total system costs varied less than the optimal capacities of the individual assets, with only a 0.7–0.8% decrease (LWR-thermal) and a 0.3% decrease (SMR-thermal) in system costs for isolated and interconnected grid constraints (Figure 3B and E and Figure 4B and E). Furthermore, our analysis shows that the change in thermal storage duration has no impact on the capacities of generation assets when dispatchable SMR or a grid interconnection is available. Our results suggest that LDS is more valuable for grid-scale applications than plant-level applications, implying that nuclear-thermal coupling may be attractive for enabling intra-day flexibility. The storage operation details for all cases are available in Appendix A (Figure A-1 through Figure A-24).

Table 11. Effect of thermal storage duration on optimal installed power/energy capacities [%].

Scenario	Case	Wind	Solar	LWR	SMR	Battery	Thermal Storage	Battery + Thermal Storage
LWR-Thermal	4/11	-2	-7	3	—	-21	100	-3
SMR-Thermal	5/12	0	0	0	0	-7	33	-3
LWR-Thermal	16*/23*	0	0	0	—	-8	-10	-9
SMR-Thermal	17*/24*	0	0	0	0	-14	500	3

* Cases with an interconnected grid constraint.

NOTE: *The effects of reduced thermal storage duration are shown as the (energy) capacity difference [%] between cases with a 10-hour duration and cases with a 5-hour duration.*

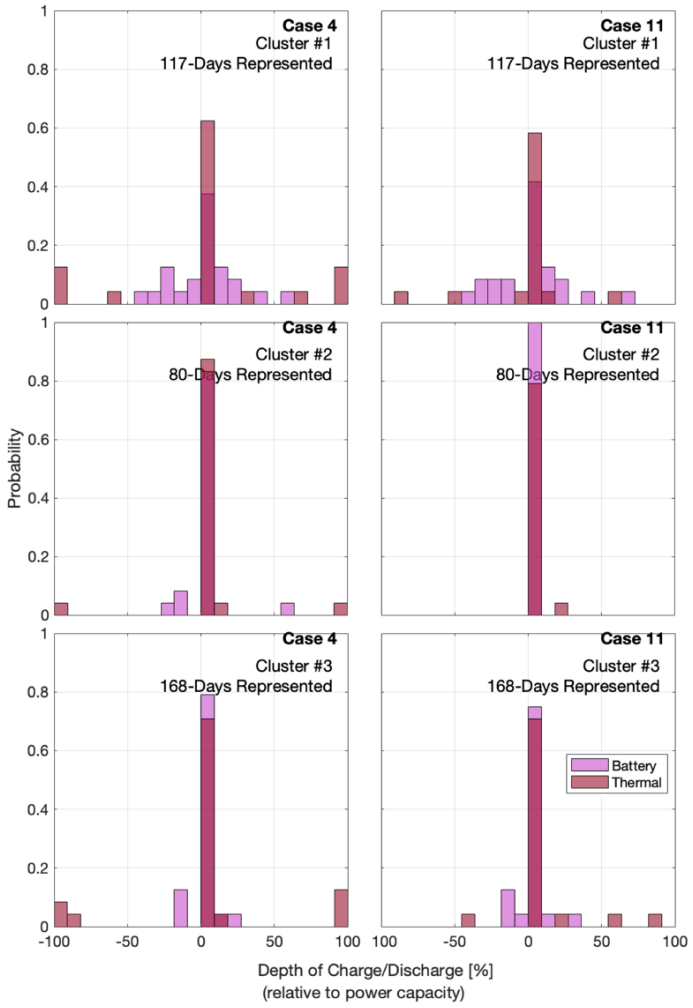

Figure 9. Impact of thermal storage duration on optimal storage operations in an isolated grid: 10 hours (left) vs. 5 hours (right).

The figure shows the distribution of hourly charge (+) and discharge (-) (relative to their own respective power capacities) for battery and thermal storage.

4. CONCLUSIONS AND FUTURE WORK

This study investigated the factors driving the expansion of nuclear reactors and the adoption of advanced nuclear technologies in the transition to decarbonized energy systems. Emphasis was placed on the interplay among storage technologies, operational constraints, and variability in thermal storage duration. Our findings demonstrate that coupling an LWR to thermal storage significantly reduces system costs, even with conservative cost projections for SMRs. Such a firm and dispatchable resource is particularly advantageous for meeting reliability criteria at a macro-scale power system level. Moreover, we observed that thermal storage is more likely to compete with SMRs and inter-regional interconnection in providing flexibility for mid-term imbalances (5–10 hours). Finally, we noted that a monetary penalty has a deterministic impact on least-cost portfolios, and future work can explore the value of extreme events in tailoring penalty functions for unmet demand.

5. ACKNOWLEDGEMENTS

This work was performed using funding received from Battelle Energy Alliance/INL. Significant computing resources were utilized at INL's High-Performance Computing Center, which is supported by the U.S. Department of Energy's Office of Nuclear Energy and the Nuclear Science User Facilities under contract no. DE-AC07-05ID14517.

6. REFERENCES

[1] S. M. Bragg-Sitton, et al. 2020. "Flexible nuclear energy for clean energy systems." NREL/TP-6A50-77088, National Renewable Energy Laboratory (NREL), Golden, CO: 2020. https://doi.org/10.2172/1665841.

[2] E. Ingersoll, K. Gogan, J. Herter, and A. Foss. 2020. "Cost & Performance Requirements for Flexible Advanced Nuclear Plants in Future US Power Markets." *LucidCatalyst, LLC*, Cambridge, MA: 2020. https://doi.org/10.2172/1646858.

[3] P. Eash-Gates, M. M. Klemun, G. Kavlak, J. McNerney, J. Buongiorno, and J. E. Trancik. 2020. "Sources of cost overrun in nuclear power plant construction call for a new approach to engineering design." *Joule* 4, no. 11 (Nov. 2020): pp. 2348-2373. https://doi.org/10.1016/j.joule.2020.10.001.

[4] S.-B. Cho, X. Sun, T. Allen, and A. Foss. 2021. "Study of Storage Requirements and Costs for Shaping with Renewables and Nuclear Energy: FY21 Summary Report." Idaho Falls, ID.

[5] P. W. Talbot, et al. 2020. "Evaluation of Hybrid FPOG Applications in Regulated and Deregulated Markets Using HERON." INL/EXT-20-60968, Idaho National Laboratory, Idaho Falls, ID. https://doi.org/10.2172/1755894.

[6] I. Bromley-Dulfano, J. Florez, and M. T. Craig. 2021. "Reliability benefits of wide-area renewable energy planning across the Western United States." *Renewable Energy* 179 (Dec. 2021): pp. 1487-1499. https://doi.org/10.1016/j.renene.2021.07.095.

[7] P. W. Talbot, et al. 2020. "Correlated synthetic time series generation for energy system simulations using Fourier and ARMA signal processing." *Int J Energy Res* 44, no. 10 (Mar. 2020), pp. 8144-8155. https://doi.org/10.1002/er.5115.

[8] K. L. Frick, et al. 2019. "Evaluation of hydrogen production feasibility for a light water reactor in the midwest." INL/EXT-19-55395-Rev. 1, Idaho National Laboratory, Idaho Falls, ID. https://doi.org/10.2172/1569271.

[9] J. Zhou, H. Abdel-Khalik, P. Talbot, and C. Rabiti. 2021. "A Hybrid Energy System Workflow for Energy Portfolio Optimization." *Energies* 14, no. 15 (2021): p. 4392. https://doi.org/10.3390/en14154392.

[10] J. A. Dowling, et al. 2020. "Role of long-duration energy storage in variable renewable electricity systems." *Joule* 4, no. 9 (Sep. 2020): pp. 1907-1928. https://doi.org/10.1016/j.joule.2020.07.007.

[11] M. S. Ziegler, et al. 2019. "Storage requirements and costs of shaping renewable energy toward grid decarbonization." *Joule* 3, no. 9 (Sep 2019): pp. 2134-2153. https://doi.org/10.1016/j.joule.2019.06.012.

[12] N. Stauff, K. Biegel, T. Levin, J. Richards, A. Cuadra, and S. Kim. 2020. "Daily Market Analysis of Load Following and Storage Impact." ANL/NSE-20/44, Argonne National Laboratory, Argonne, IL. https://www.osti.gov/servlets/purl/1701718.

[13] J. Buongiorno, J. E. Parsons, D. A. Petti, and J. Parsons. 2019. "The future of nuclear energy in a carbon-constrained world." *MIT Energy Initiative.* https://energy.mit.edu/research/future-nuclear-energy-carbon-constrained-world/.

[14] A. Stein, J. Messinger, S. Wang, J. Lloyd, J. McBride, and R. Franovich. 2022. "Advancing Nuclear Energy - Evaluating Deployment, Investment, and Impact in America's Clean Energy Future." *Breakthrough Institute*, Oakland, CA. [Online] https://thebreakthrough.imgix.net/Advancing-Nuclear-Energy_v3-compressed.pdf.

[15] R. Armstrong, Y.-M. Chiang, H. Gruenspecht, and F. Brushett. 2022. "The Future of Energy Storage." *MIT Energy Initiative*. https://energy.mit.edu/publication/the-future-of-energy-storage/.

[16] P. W. Talbot, A. Gairola, P. Prateek, A. Alfonsi, C. Rabiti, and R. D. Boardman. 2019. "HERON as a Tool for LWR Market Interaction in a Deregulated Market." Idaho National Laboratory, Idaho Falls, ID. https://doi.org/10.2172/1581179.

[17] F. J. De Sisternes, J. D. Jenkins, and A. Botterud. "The value of energy storage in decarbonizing the electricity sector." *Applied Energy* 175 (Aug. 2016): pp. 368-379. https://doi.org/10.1016/j.apenergy.2016.05.014.

[18] L. Duan, R. Petroski, L. Wood, and K. Caldeira. 2022. "Stylized least-cost analysis of flexible nuclear power in deeply decarbonized electricity systems considering wind and solar resources worldwide." *Nature Energy* 7, no. 3 (2022): pp. 260-269. http://dx.doi.org/10.1038/s41560-022-00979-x.

[19] T. Baker, A. Epiney, C. Rabiti, and E. Shittu. 2018. "Optimal sizing of flexible nuclear hybrid energy system components considering wind volatility." *Applied Energy* 212 (Feb. 2018): pp. 498-508. https://doi.org/10.1016/j.apenergy.2017.12.061.

[20] A. Epiney, C. Rabiti, P. Talbot, and A. Alfonsi. 2020. "Economic analysis of a nuclear hybrid energy system in a stochastic environment including wind turbines in an electricity grid." *Applied Energy* 260 (Feb. 2020): p. 114227. https://doi.org/10.1016/j.apenergy.2019.114227.

[21] M. J. Sullivan, M. Mercurio, and J. Schellenberg. 2009. "Estimated value of service reliability for electric utility customers in the United States." LBNL-2132E, Lawrence Berkeley National Laboratory, Berkeley, CA. https://doi.org/10.2172/963320.

[22] NREL. 2010. "Simple Levelized Cost of Energy (LCOE) Calculator Documentation." *National Renewable Energy Laboratory*. https://www.nrel.gov/analysis/tech-lcoe-documentation.html.

[23] M. Sufyan, N. Abd Rahim, C. Tan, M. A. Muhammad, and S. R. Sheikh Raihan. 2019. "Optimal sizing and energy scheduling of isolated microgrid considering the battery lifetime degradation." *plos one* 14, no. 2 (Feb. 2019): p. 0211642. https://doi.org/10.1371/journal.pone.0211642.

[24] A. Millner. 2010. "Modeling lithium ion battery degradation in electric vehicles." in *2010 IEEE Conference on Innovative Technologies for an Efficient and Reliable Electricity Supply*, Waltham, MA, USA: (Sep.2010): pp. 349-356. https://doi.org/10.1109/CITRES.2010.5619782.

[25] N. A. Sepulveda, J. D. Jenkins, F. J. de Sisternes, and R. K. Lester. 2018. "The role of firm low-carbon electricity resources in deep decarbonization of power generation." *Joule* 2, no. 11 (Nov. 2018): pp. 2403-2420. https://doi.org/10.1016/j.joule.2018.08.006.

[26] R. M. Saeed, et al 2022. "Multilevel Analysis, Design, and Modeling of Coupling Advanced Nuclear Reactors and Thermal Energy Storage in an Integrated Energy System." INL/RPT-22-69214-Rev000, Idaho National Laboratory, Idaho Falls, ID. https://doi.org/10.2172/1890160.

Appendix A
Supplementary Figures

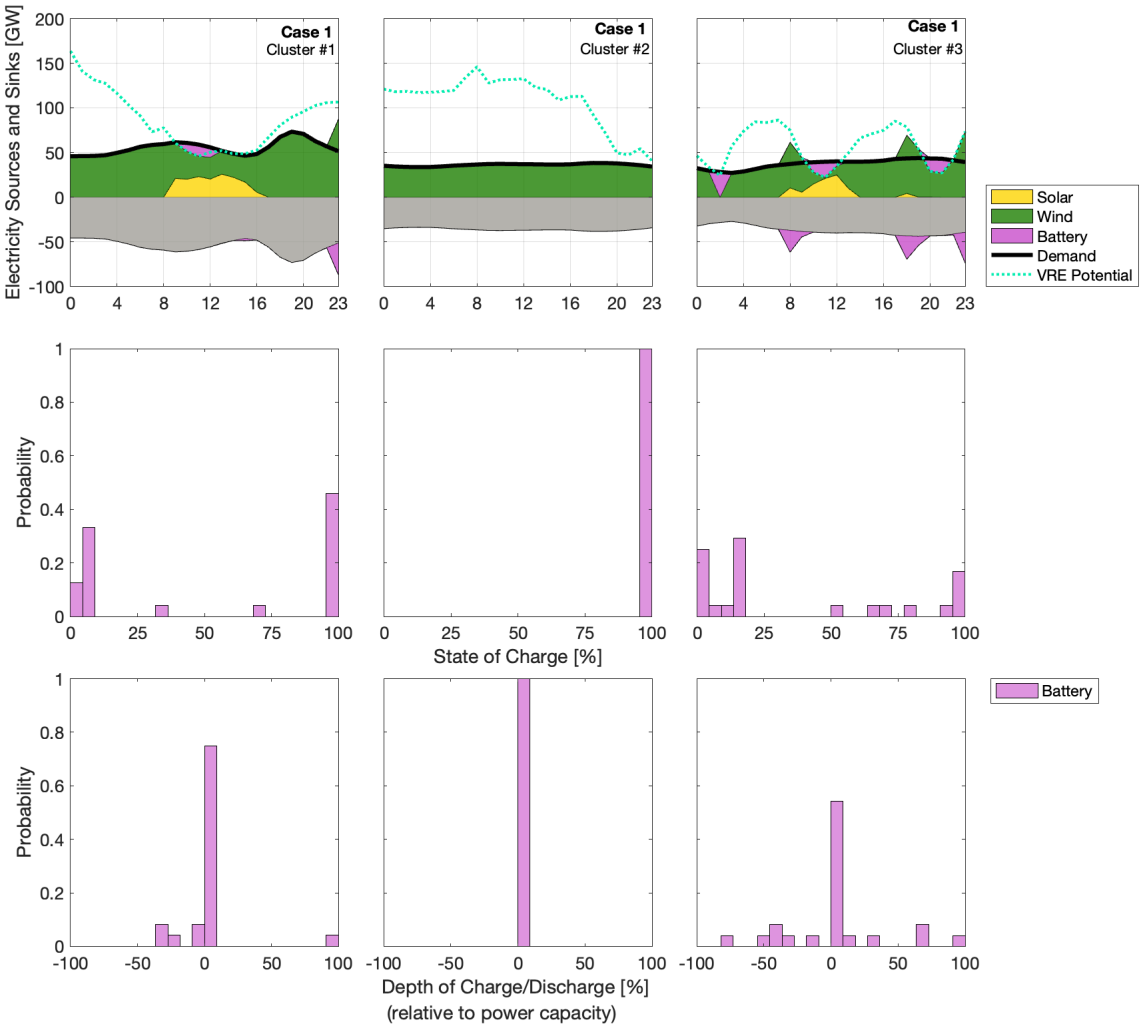

Figure A-1. Hourly dispatch of optimal generation mix with 1-day temporal extent, as obtained through cost-minimization, showcasing the least-cost portfolio. This figure shows 1 day of dispatch for each of three clusters, along with the corresponding hourly charge (+) and discharge (-) (relative to their own respective power capacities) for battery storage.

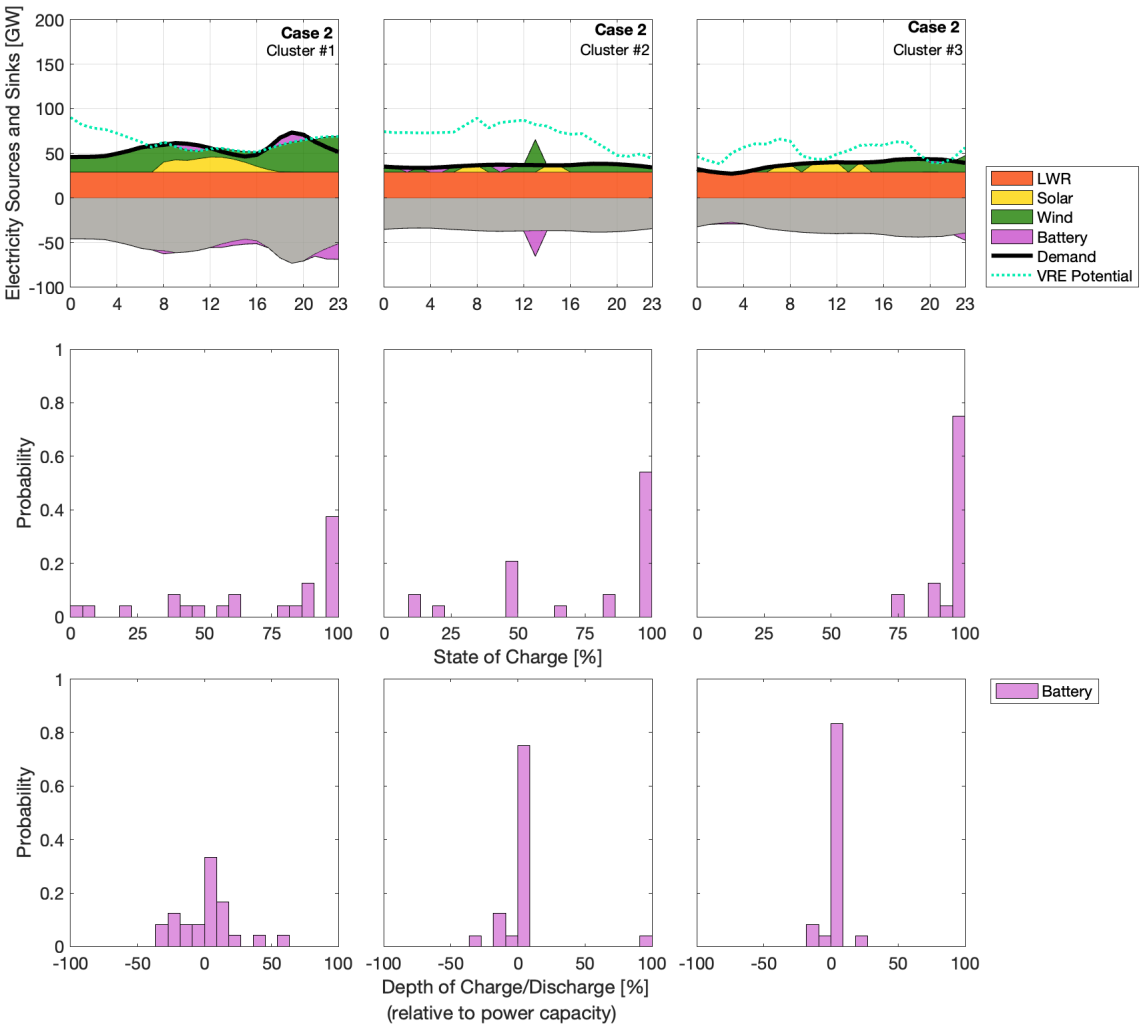

Figure A-2. Hourly dispatch of optimal generation mix with 1-day temporal extent, as obtained through cost-minimization, showcasing the least-cost portfolio. This figure shows 1 day of dispatch for each of three clusters, along with the corresponding hourly charge (+) and discharge (-) (relative to their own respective power capacities) for battery storage.

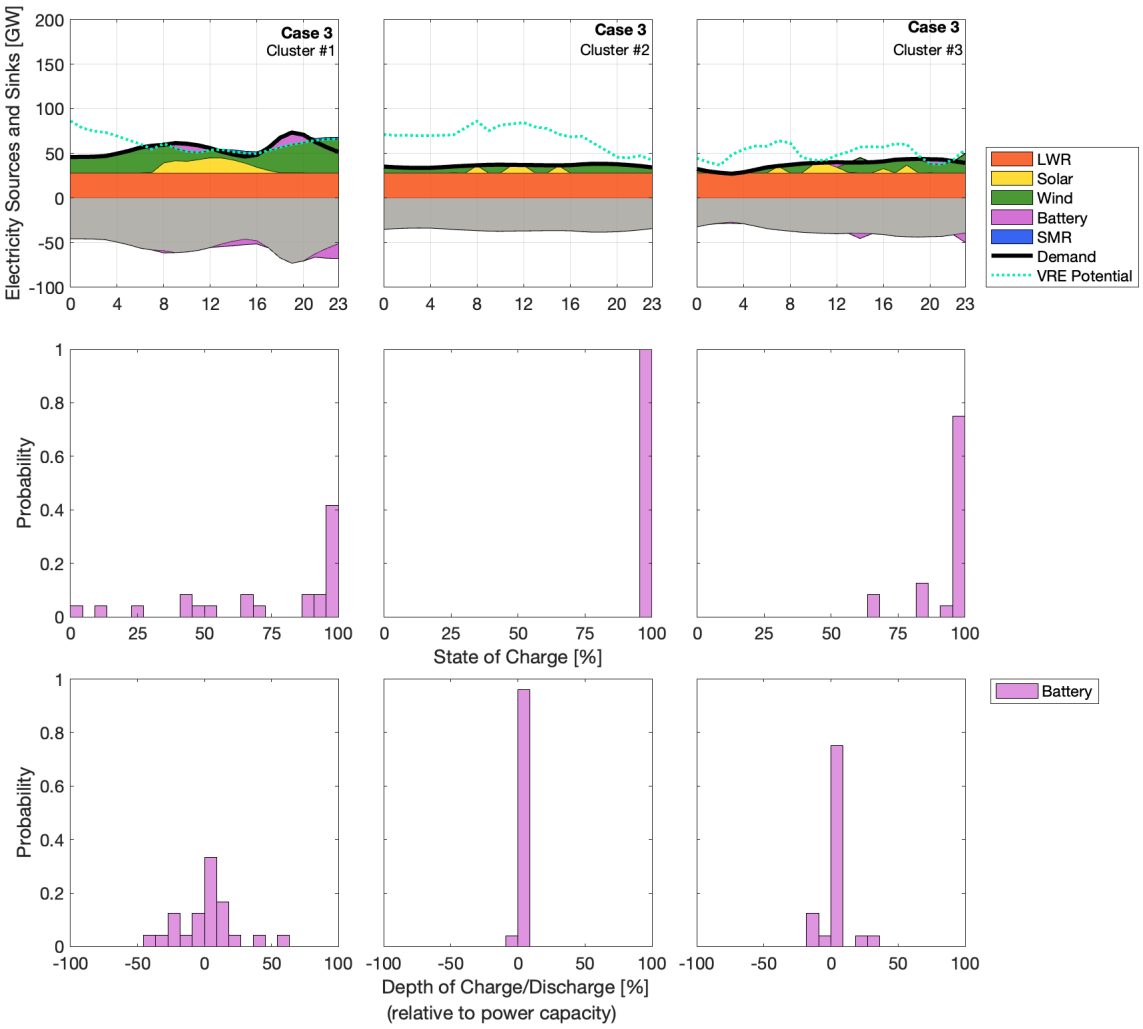

Figure A-3. Hourly dispatch of optimal generation mix with 1-day temporal extent, as obtained through cost-minimization, showcasing the least-cost portfolio. This figure shows 1 day of dispatch for each of three clusters with the corresponding hourly charge (+) and discharge (-) (relative to their own respective power capacities) for battery storage.

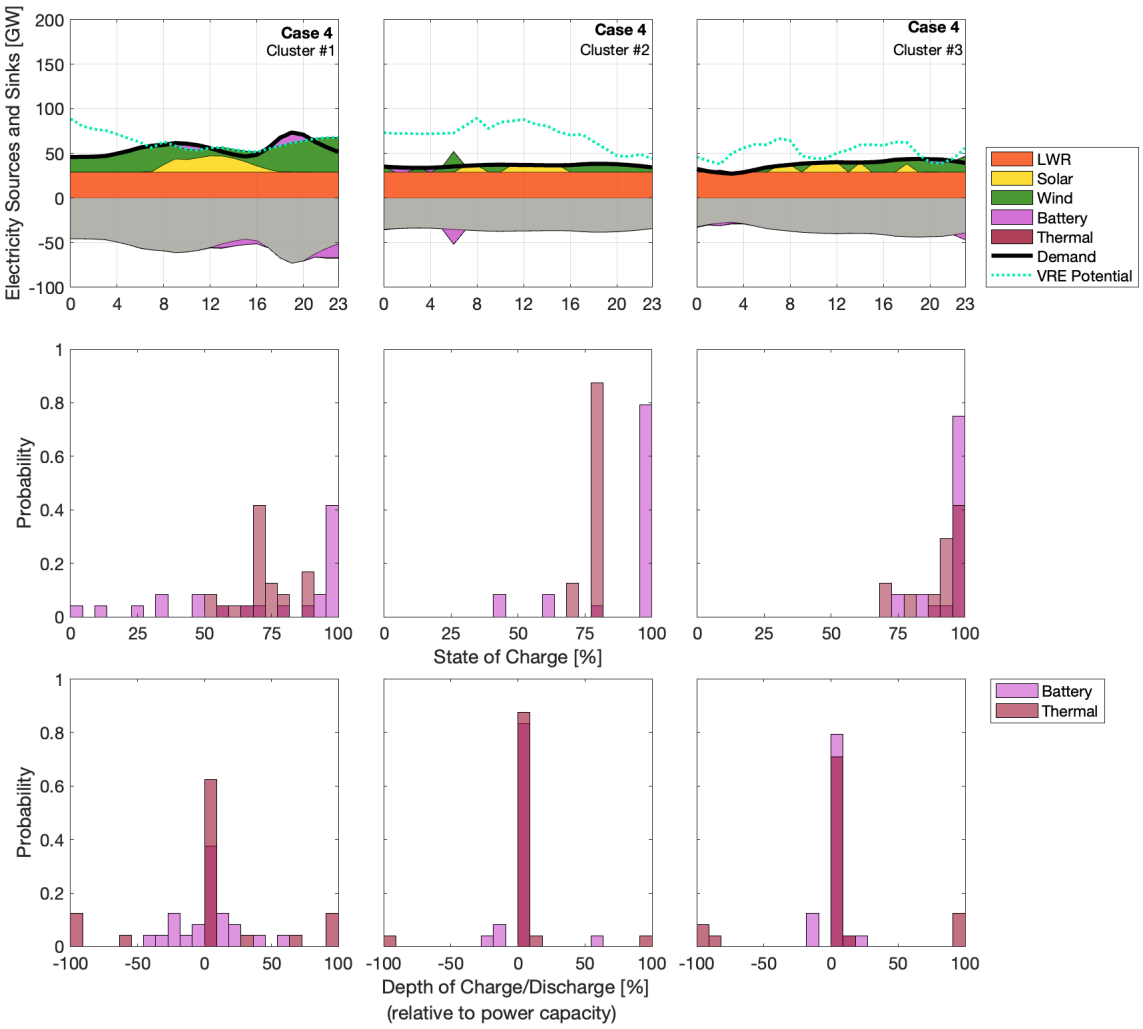

Figure A-4. Hourly dispatch of optimal generation mix with 1-day temporal extent, as obtained through cost-minimization, showcasing the least-cost portfolio. This figure shows 1 day of dispatch for each of three clusters, along with the corresponding hourly charge (+) and discharge (-) (relative to their own respective power capacities) for battery and thermal storage.

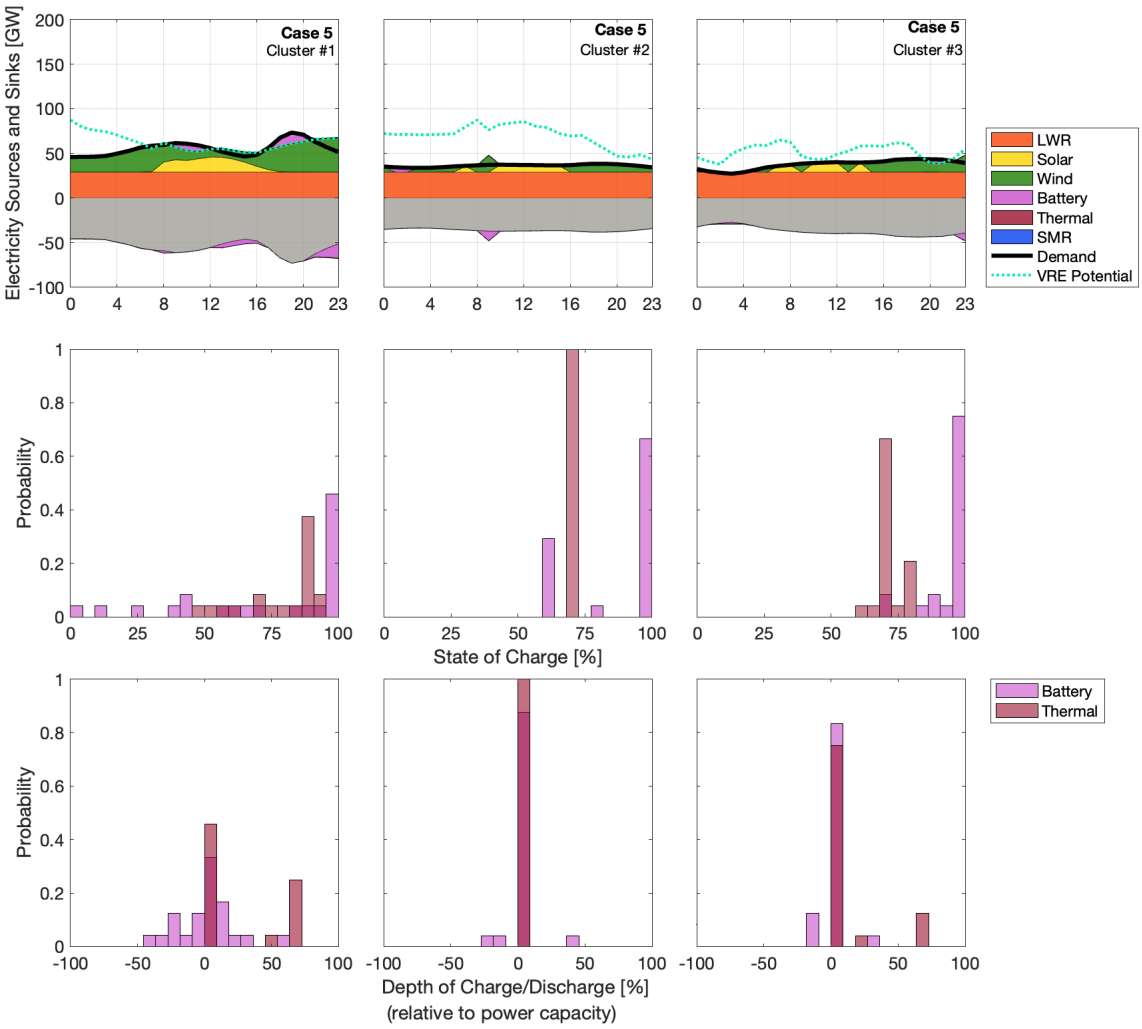

Figure A-5. Hourly dispatch of optimal generation mix with 1-day temporal extent, as obtained through cost-minimization, showcasing the least-cost portfolio. This figure shows 1 day of dispatch for each of three clusters, along with the corresponding hourly charge (+) and discharge (-) (relative to their own respective power capacities) for battery and thermal storage.

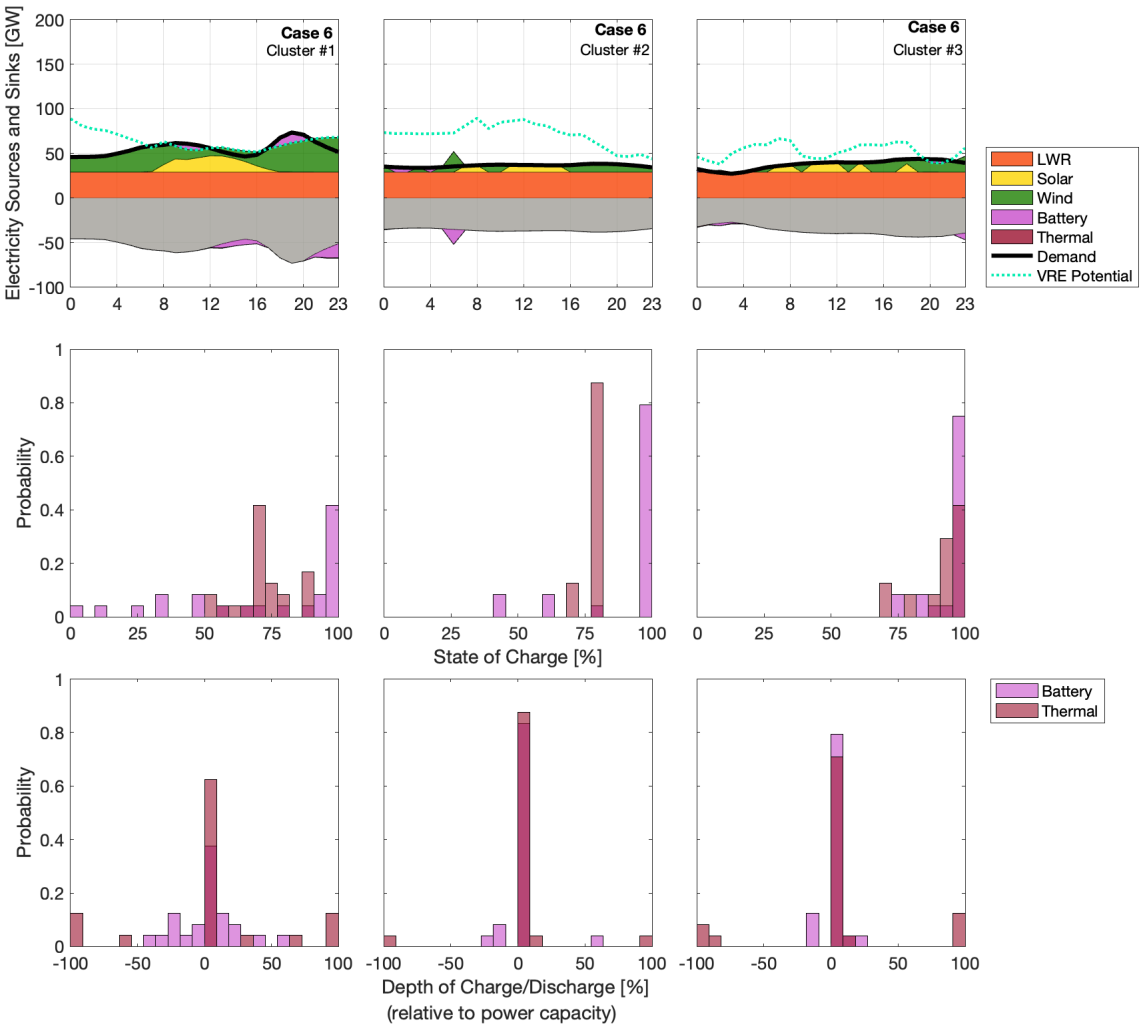

Figure A-6. Hourly dispatch of optimal generation mix with 1-day temporal extent, as obtained through cost-minimization, showcasing the least-cost portfolio. This figure shows 1 day of dispatch for each of three clusters, along with the corresponding hourly charge (+) and discharge (-) (relative to their own respective power capacities) for battery and thermal storage.

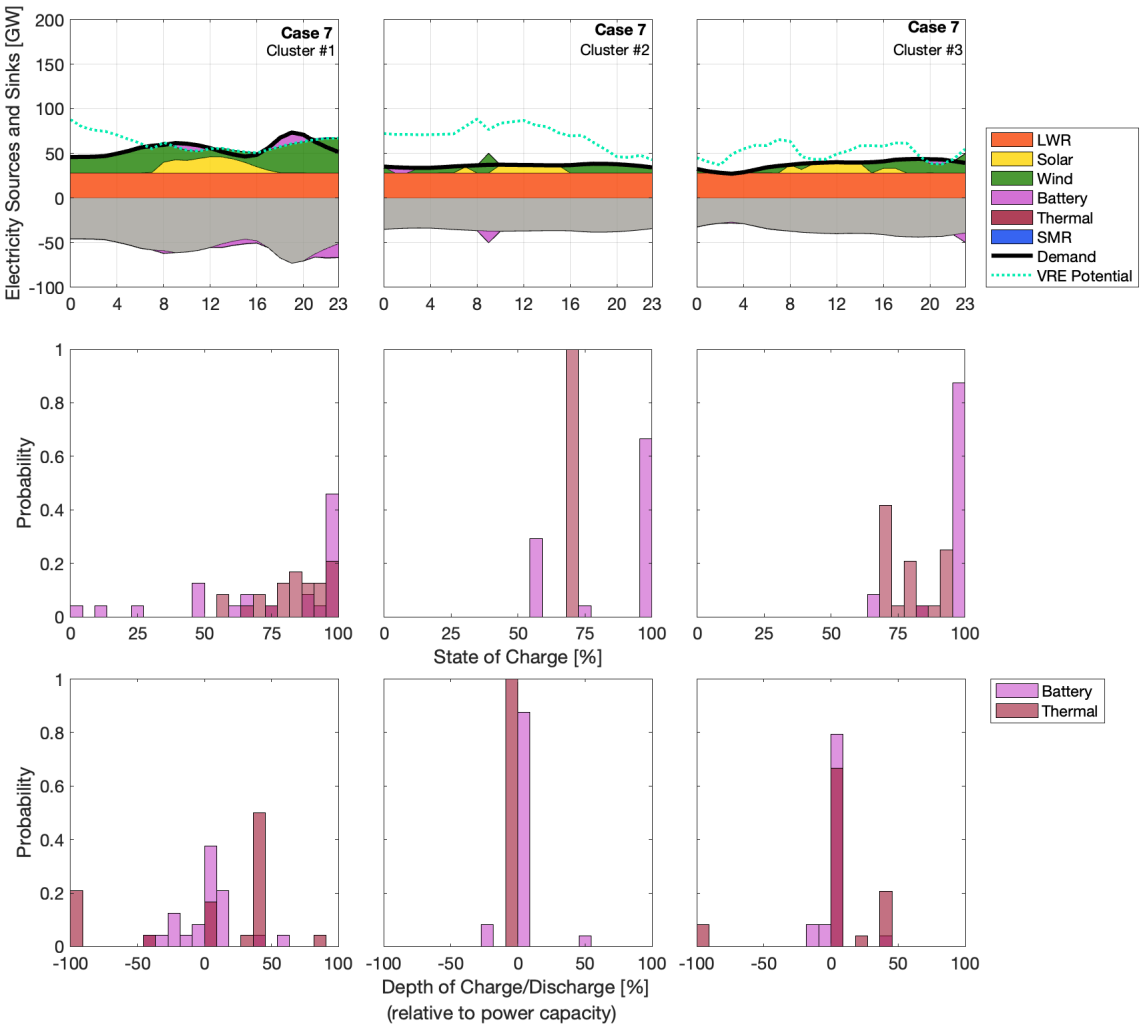

Figure A-7. Hourly dispatch of optimal generation mix with 1-day temporal extent, as obtained through cost-minimization, showcasing the least-cost portfolio. This figure shows 1 day of dispatch for each of three clusters, along with the corresponding hourly charge (+) and discharge (-) (relative to their own respective power capacities) for battery and thermal storage.

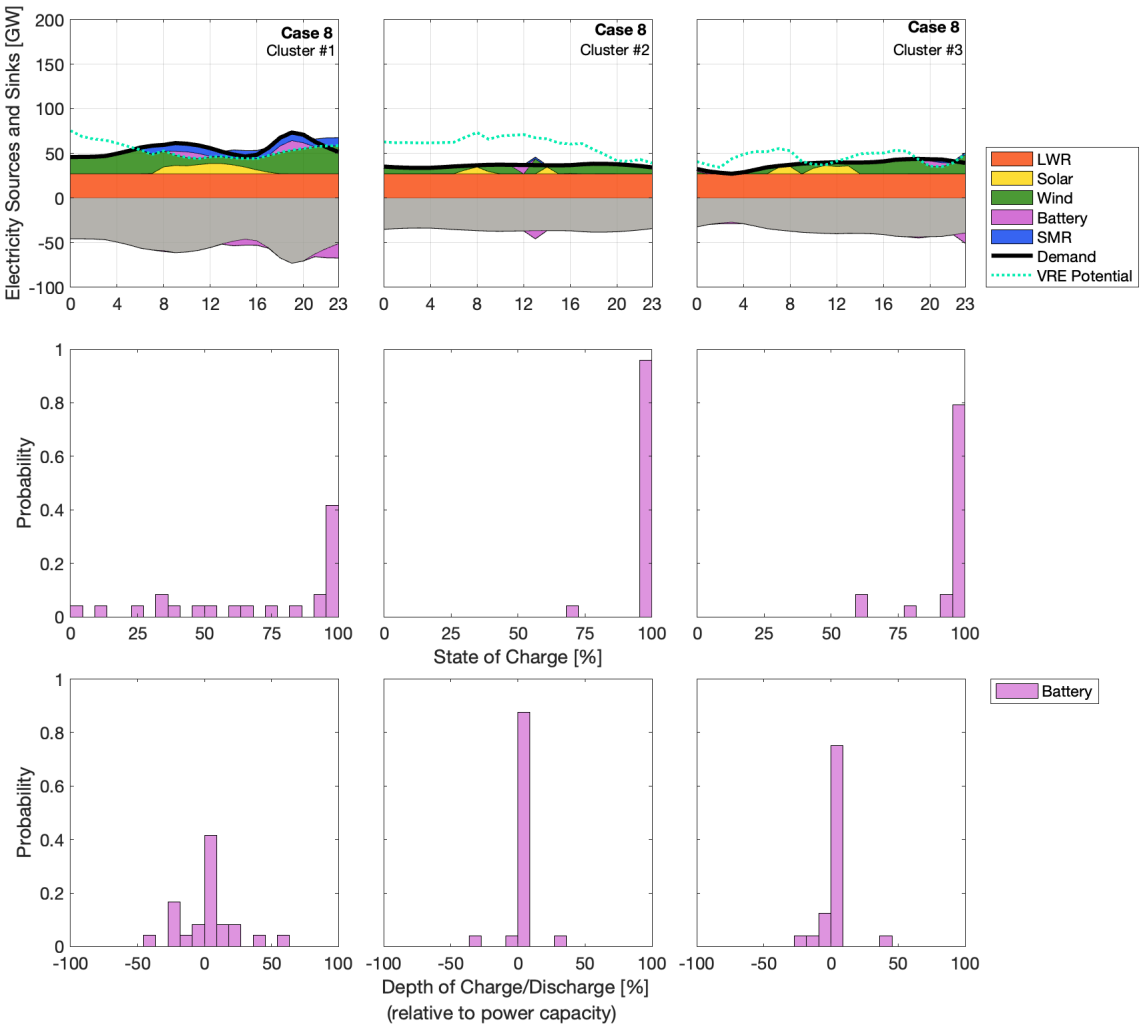

Figure A-8. Hourly dispatch of optimal generation mix with 1-day temporal extent, as obtained through cost-minimization, showcasing the least-cost portfolio. This figure shows 1 day of dispatch for each of three clusters, along with the corresponding hourly charge (+) and discharge (-) (relative to their own respective power capacities) for battery storage.

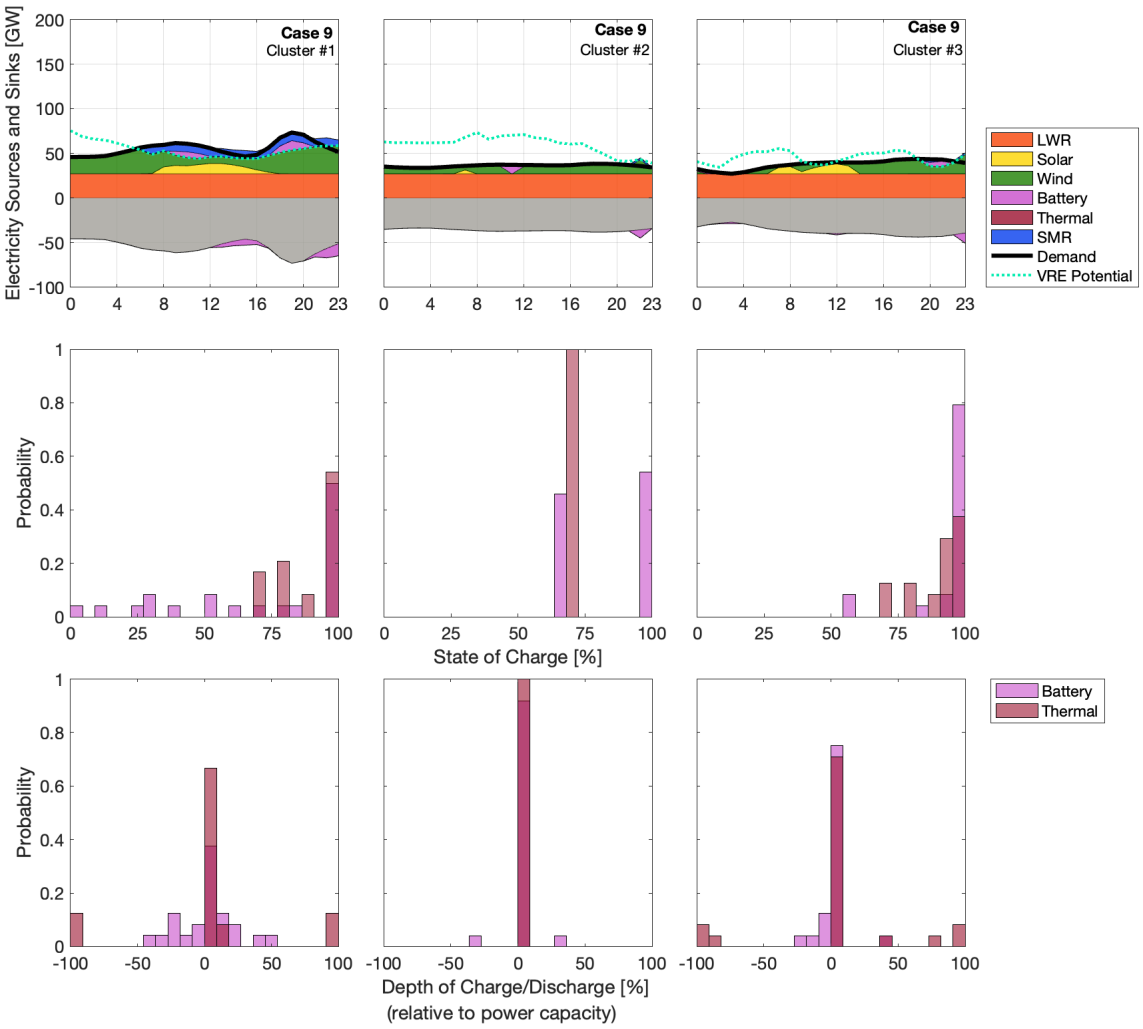

Figure A-9. Hourly dispatch of optimal generation mix with 1-day temporal extent, as obtained through cost-minimization, showcasing the least-cost portfolio. This figure shows 1 day of dispatch for each of three clusters, along with the corresponding hourly charge (+) and discharge (-) (relative to their own respective power capacities) for battery and thermal storage.

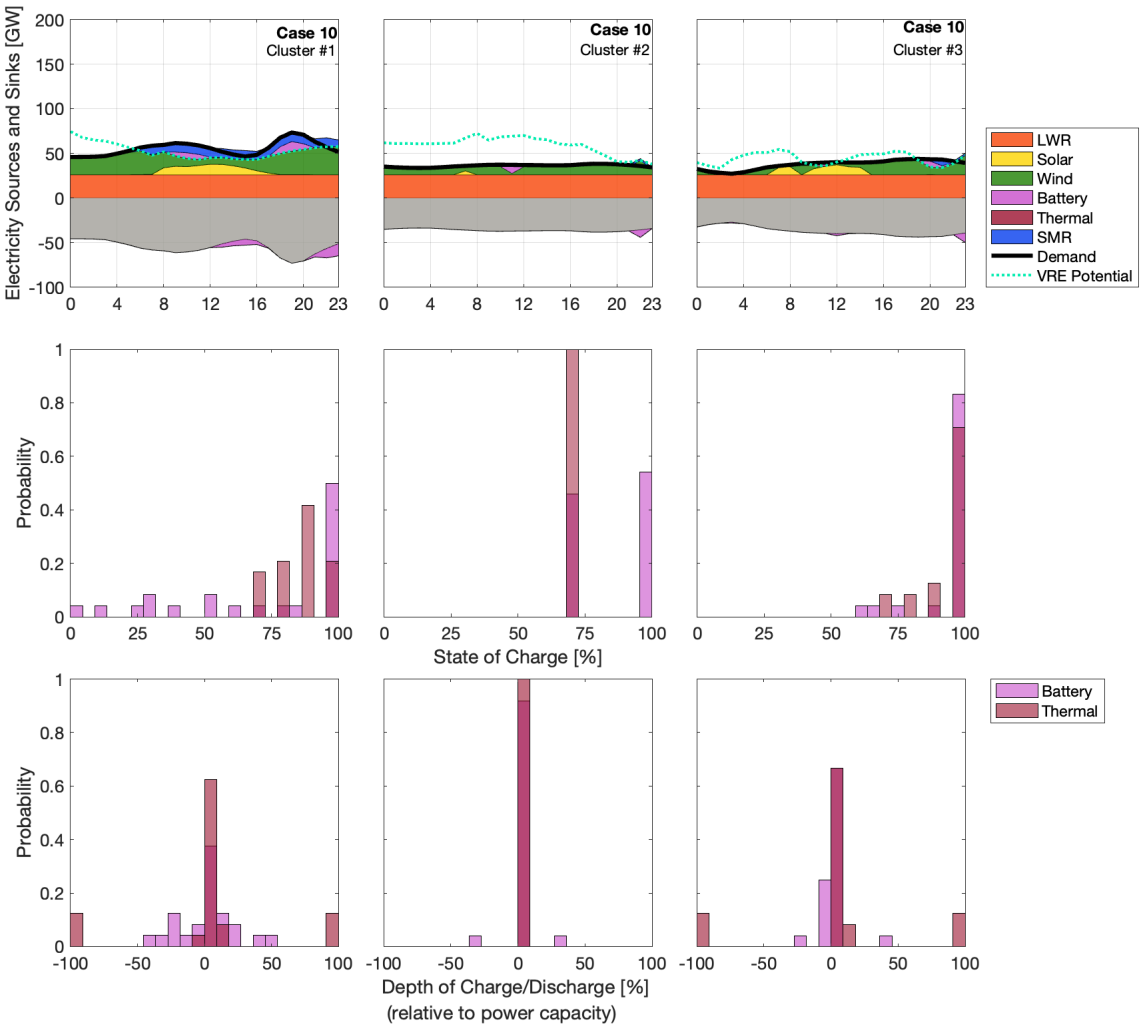

Figure A-10. Hourly dispatch of optimal generation mix with 1-day temporal extent, as obtained through cost-minimization, showcasing the least-cost portfolio. This figure shows 1 day of dispatch for each of three clusters, along with the corresponding hourly charge (+) and discharge (-) (relative to their own respective power capacities) for battery and thermal storage.

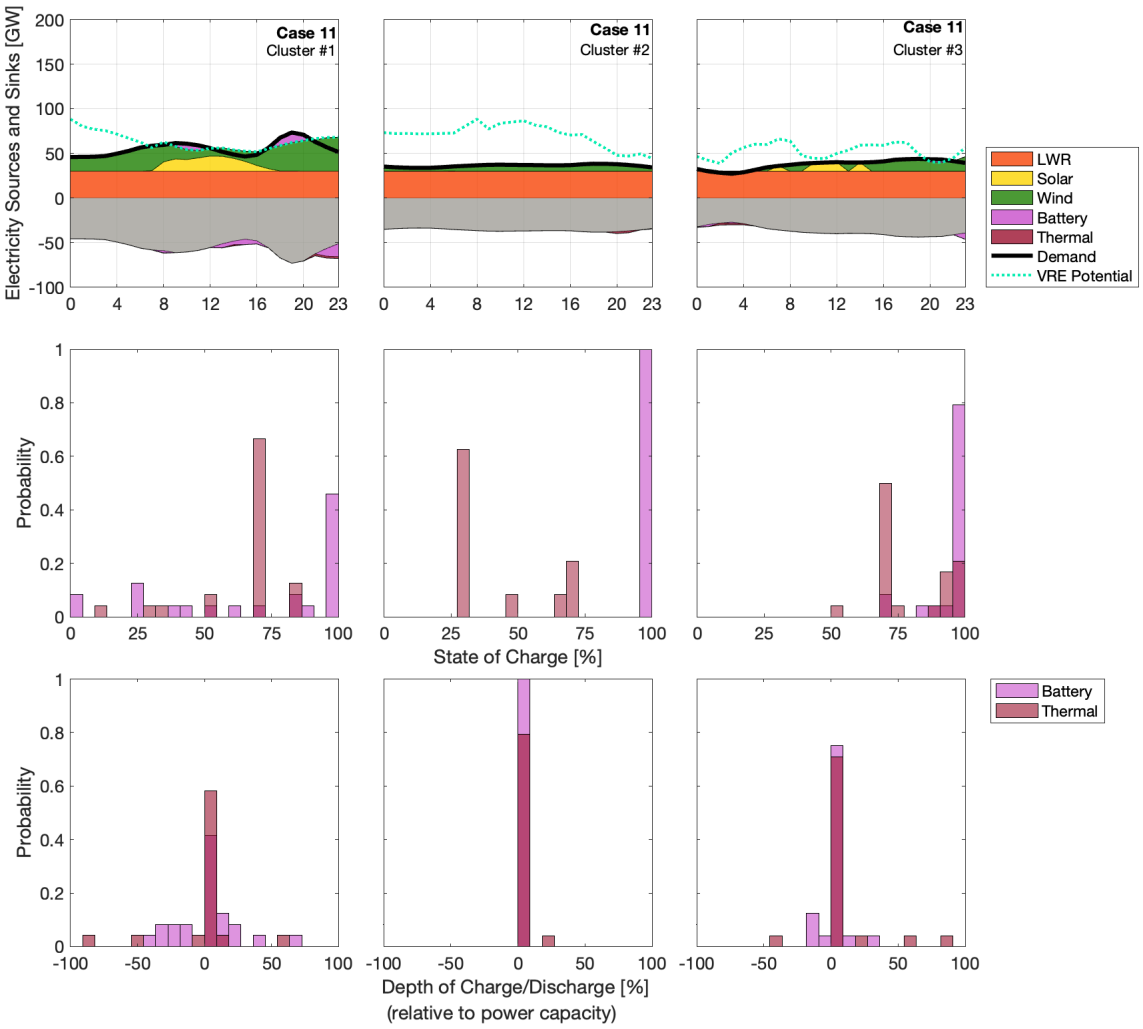

Figure A-11. Hourly dispatch of optimal generation mix with 1-day temporal extent, as obtained through cost-minimization, showcasing the least-cost portfolio. This figure shows 1 day of dispatch for each of three clusters, along with the corresponding hourly charge (+) and discharge (-) (relative to their own respective power capacities) for battery and thermal storage.

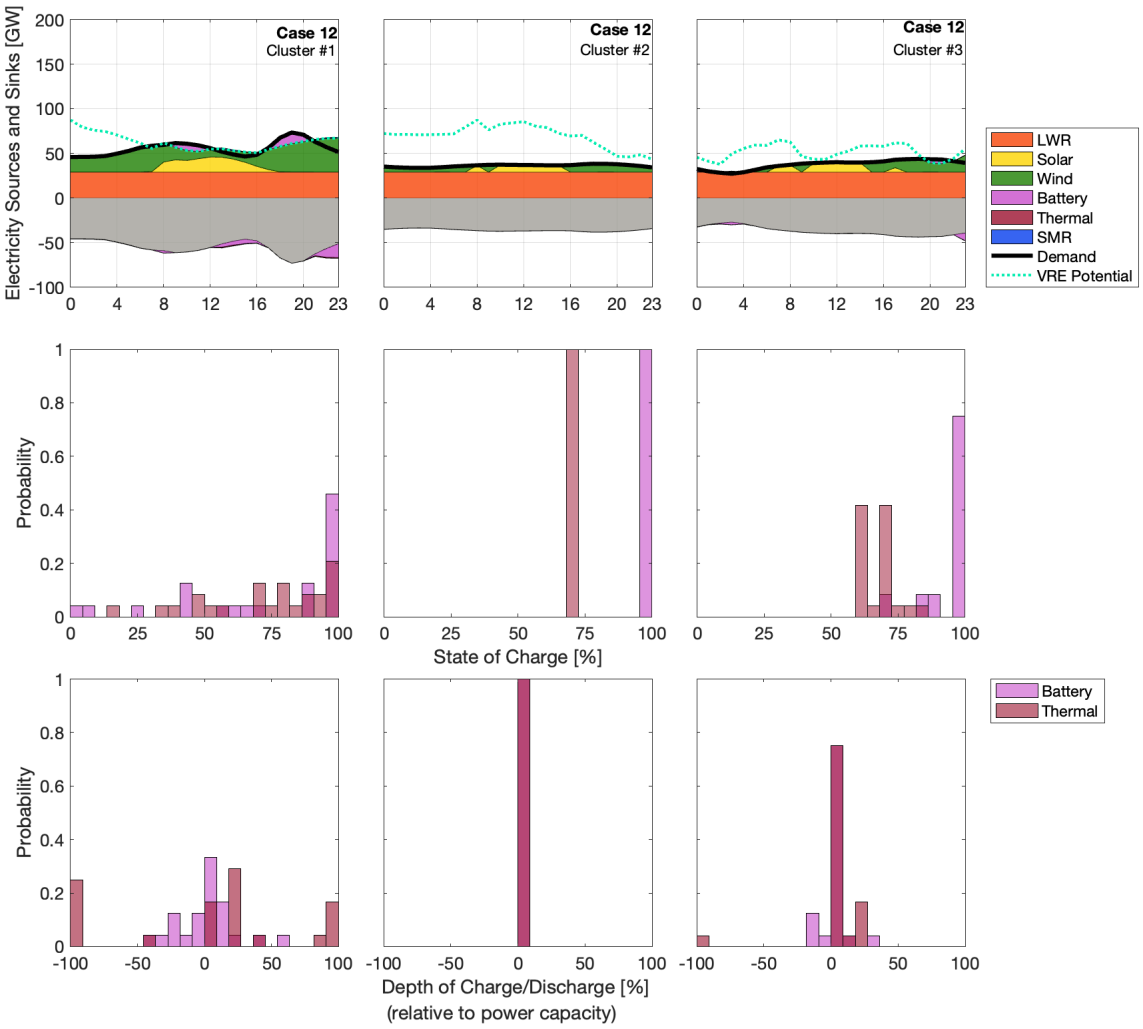

Figure A-12. Hourly dispatch of optimal generation mix with 1-day temporal extent, as obtained through cost-minimization, showcasing the least-cost portfolio. This figure shows 1 day of dispatch for each of three clusters, along with the corresponding hourly charge (+) and discharge (-) (relative to their own respective power capacities) for battery and thermal storage.

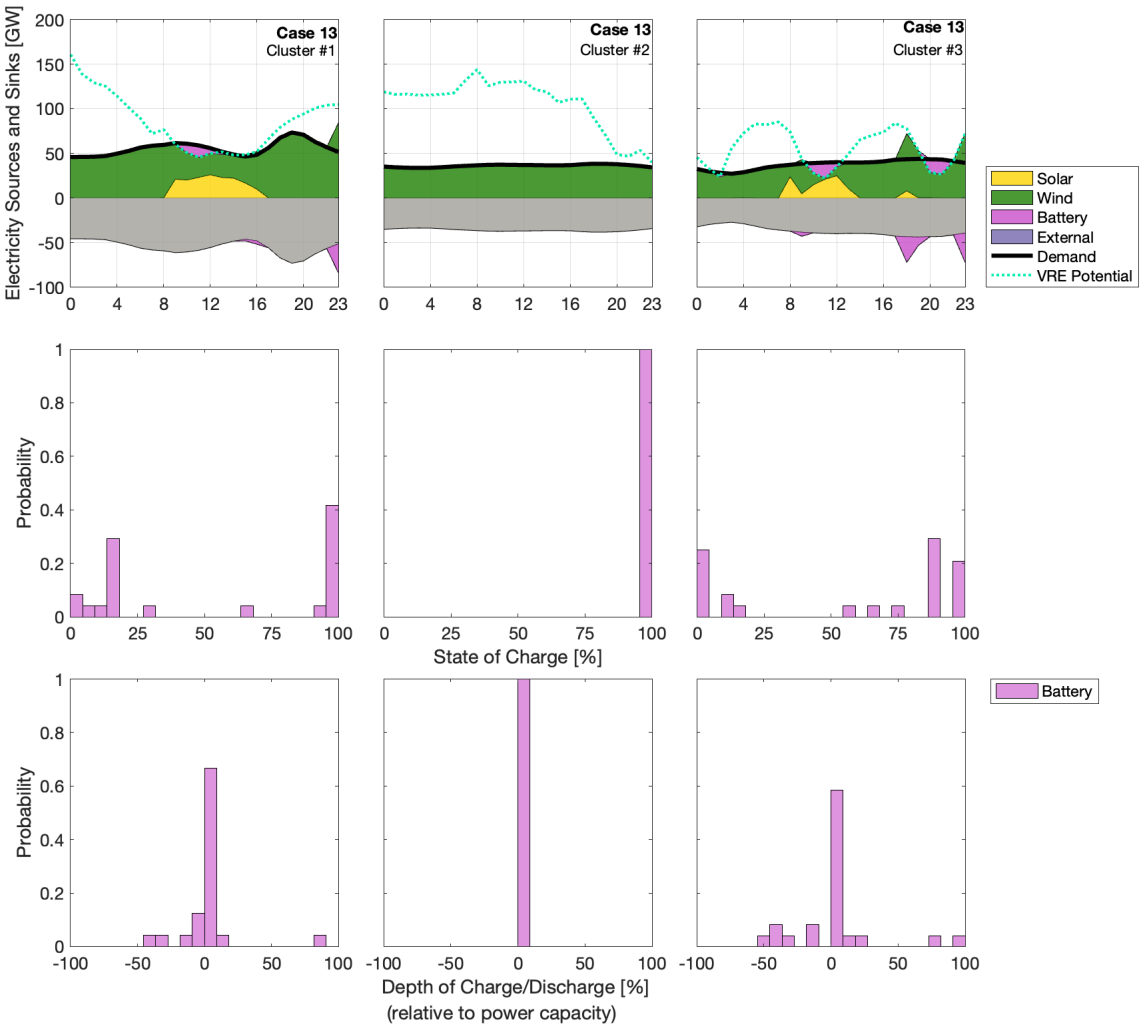

Figure A-13. Hourly dispatch of optimal generation mix with 1-day temporal extent, as obtained through cost-minimization, showcasing the least-cost portfolio. This figure shows 1 day of dispatch for each of three clusters, along with the corresponding hourly charge (+) and discharge (-) (relative to their own respective power capacities) for battery storage.

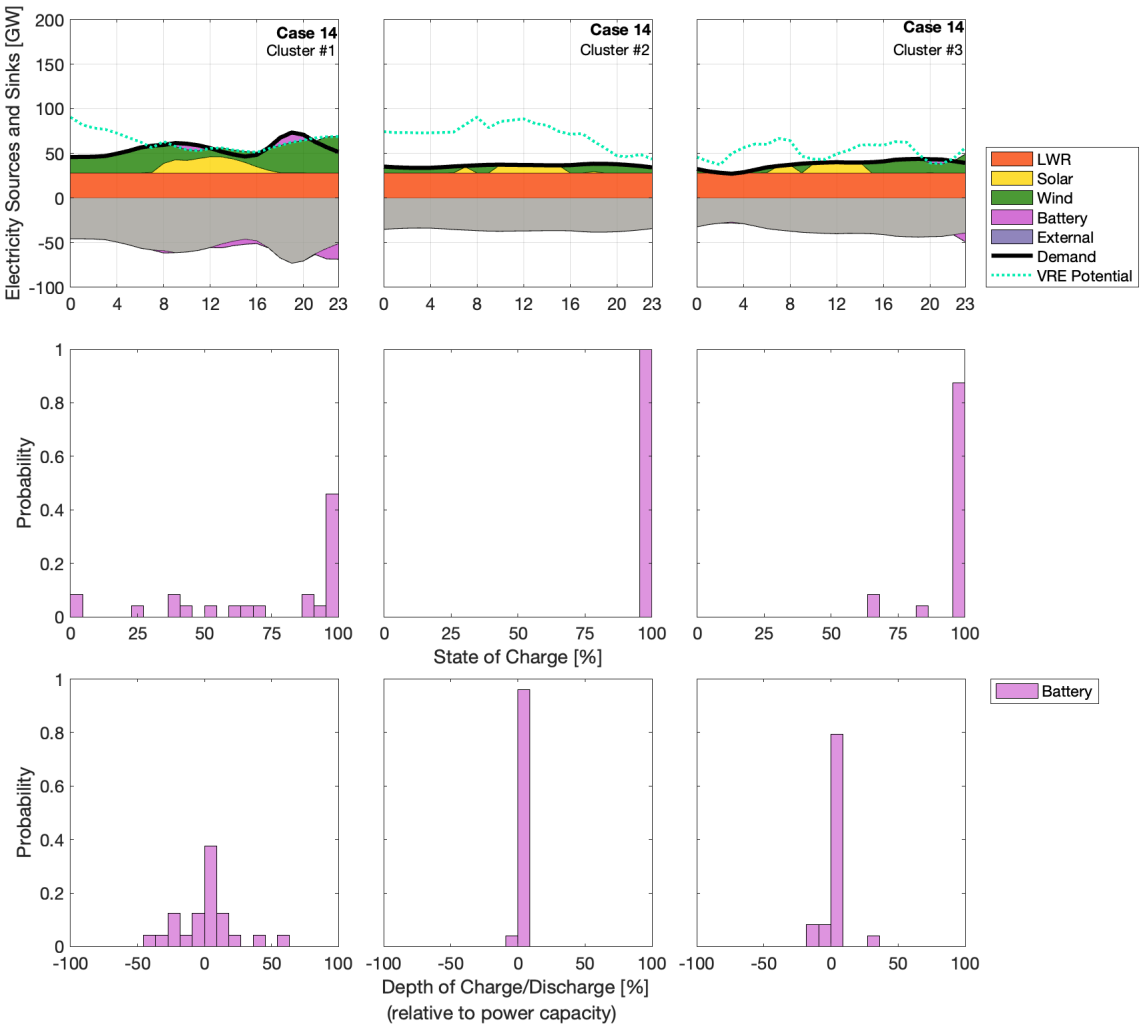

Figure A-14. Hourly dispatch of optimal generation mix with 1-day temporal extent, as obtained through cost-minimization, showcasing the least-cost portfolio. This figure shows 1 day of dispatch for each of three clusters, along with the corresponding hourly charge (+) and discharge (-) (relative to their own respective power capacities) for battery storage.

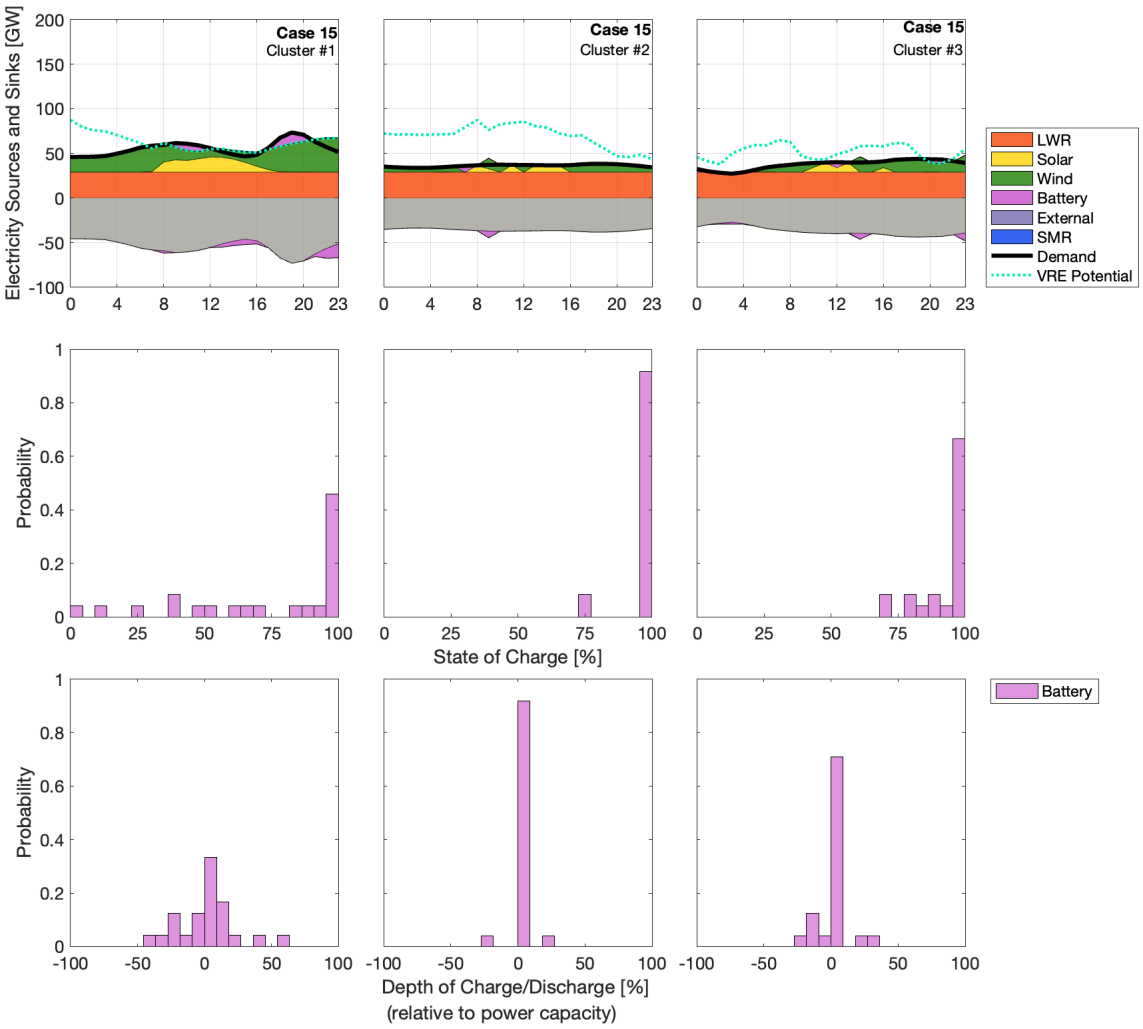

Figure A-15. Hourly dispatch of optimal generation mix with 1-day temporal extent, as obtained through cost-minimization, showcasing the least-cost portfolio. This figure shows 1 day of dispatch for each of three clusters, along with the corresponding hourly charge (+) and discharge (-) (relative to their own respective power capacities) for battery storage.

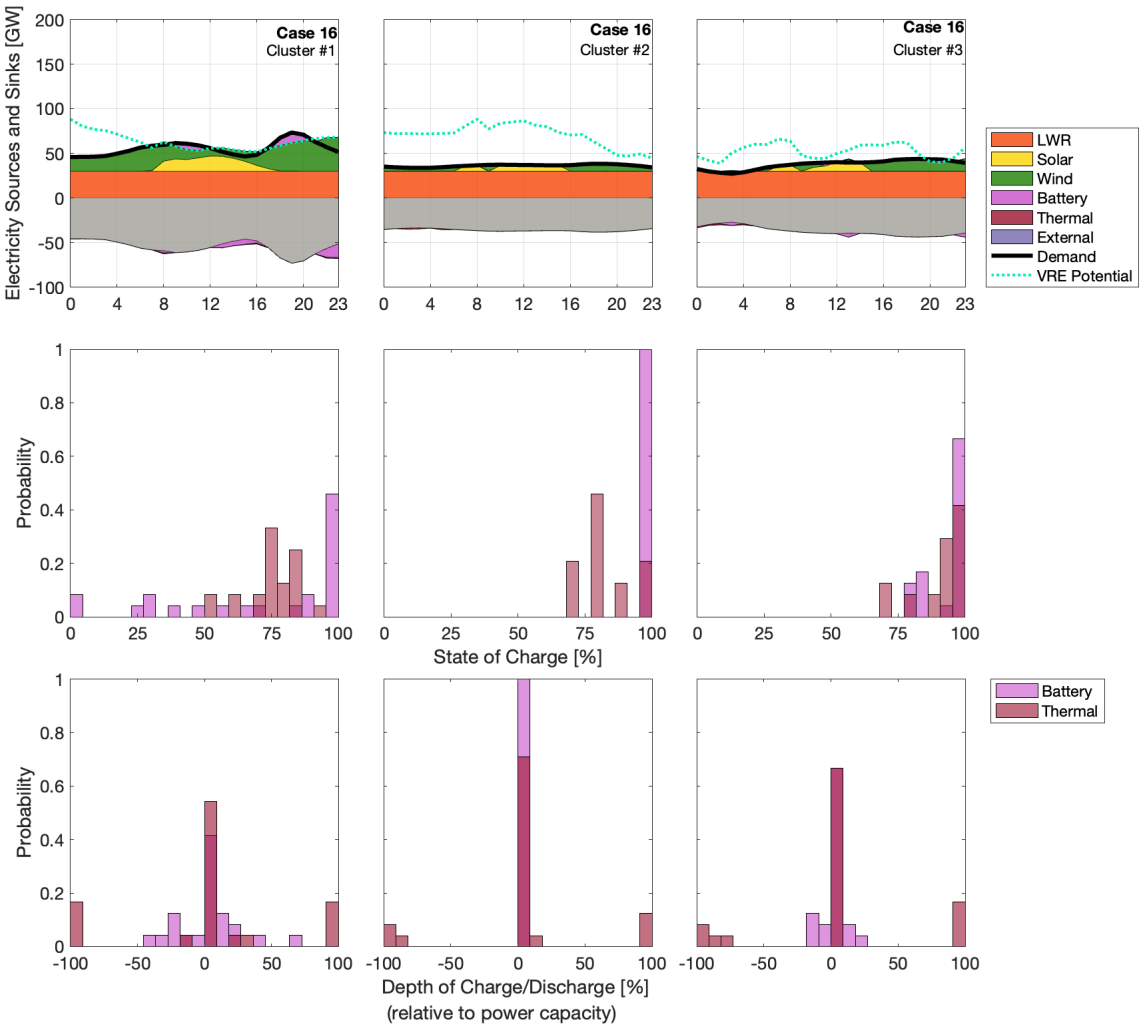

Figure A-16. Hourly dispatch of optimal generation mix with 1-day temporal extent, as obtained through cost-minimization, showcasing the least-cost portfolio. This figure shows 1 day of dispatch for each of three clusters, along with the corresponding hourly charge (+) and discharge (-) (relative to their own respective power capacities) for battery and thermal storage.

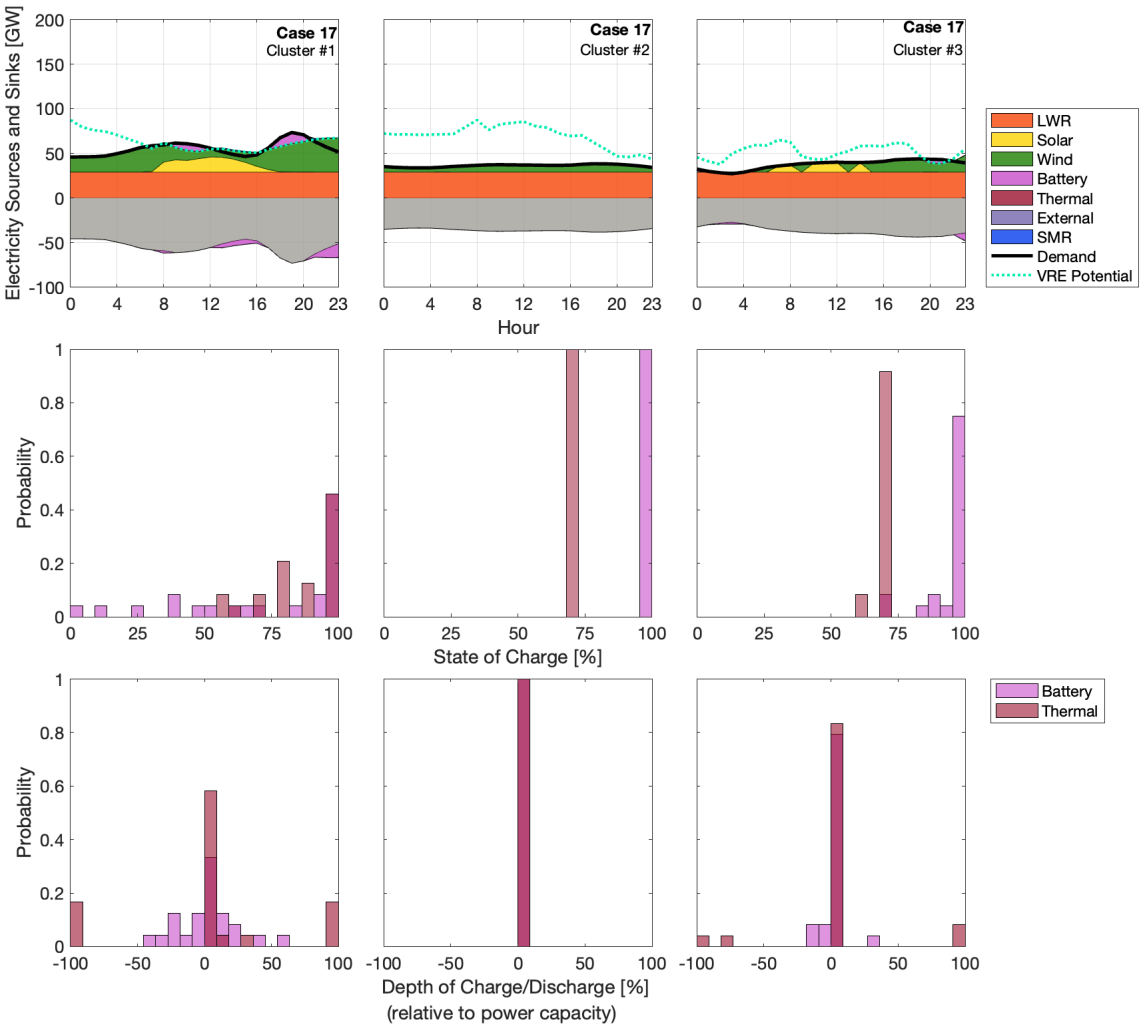

Figure A-17. Hourly dispatch of optimal generation mix with 1-day temporal extent, as obtained through cost-minimization, showcasing the least-cost portfolio. This figure shows 1 day of dispatch for each of three clusters, along with the corresponding hourly charge (+) and discharge (-) (relative to their own respective power capacities) for battery and thermal storage.

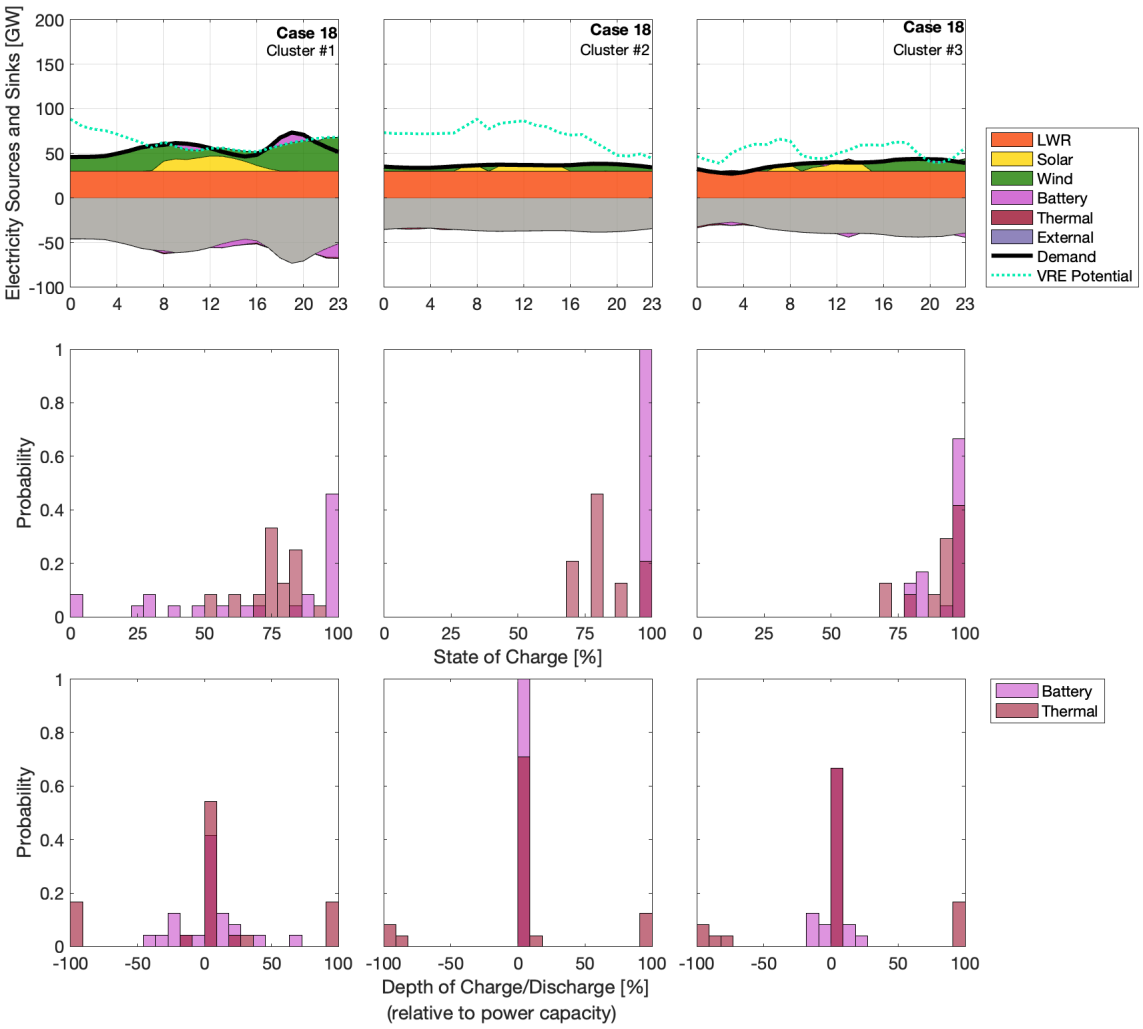

Figure A-18. Hourly dispatch of optimal generation mix with 1-day temporal extent, as obtained through cost-minimization, showcasing the least-cost portfolio. This figure shows 1 day of dispatch for each of three clusters, along with the corresponding hourly charge (+) and discharge (-) (relative to their own respective power capacities) for battery and thermal storage.

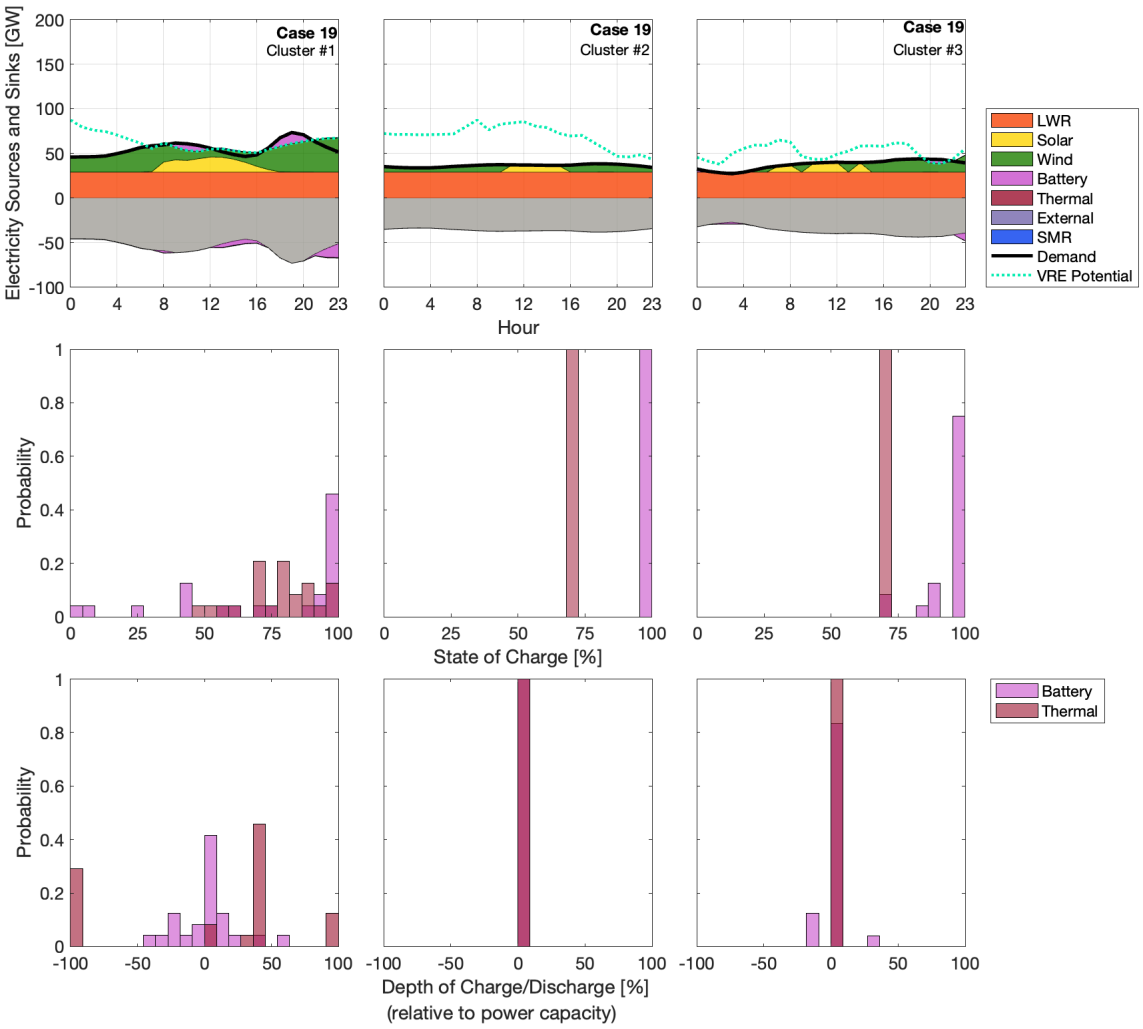

Figure A-19. Hourly dispatch of optimal generation mix with 1-day temporal extent, as obtained through cost-minimization, showcasing the least-cost portfolio. This figure shows 1 day of dispatch for each of three clusters, along with the corresponding hourly charge (+) and discharge (-) (relative to their own respective power capacities) for battery and thermal storage.

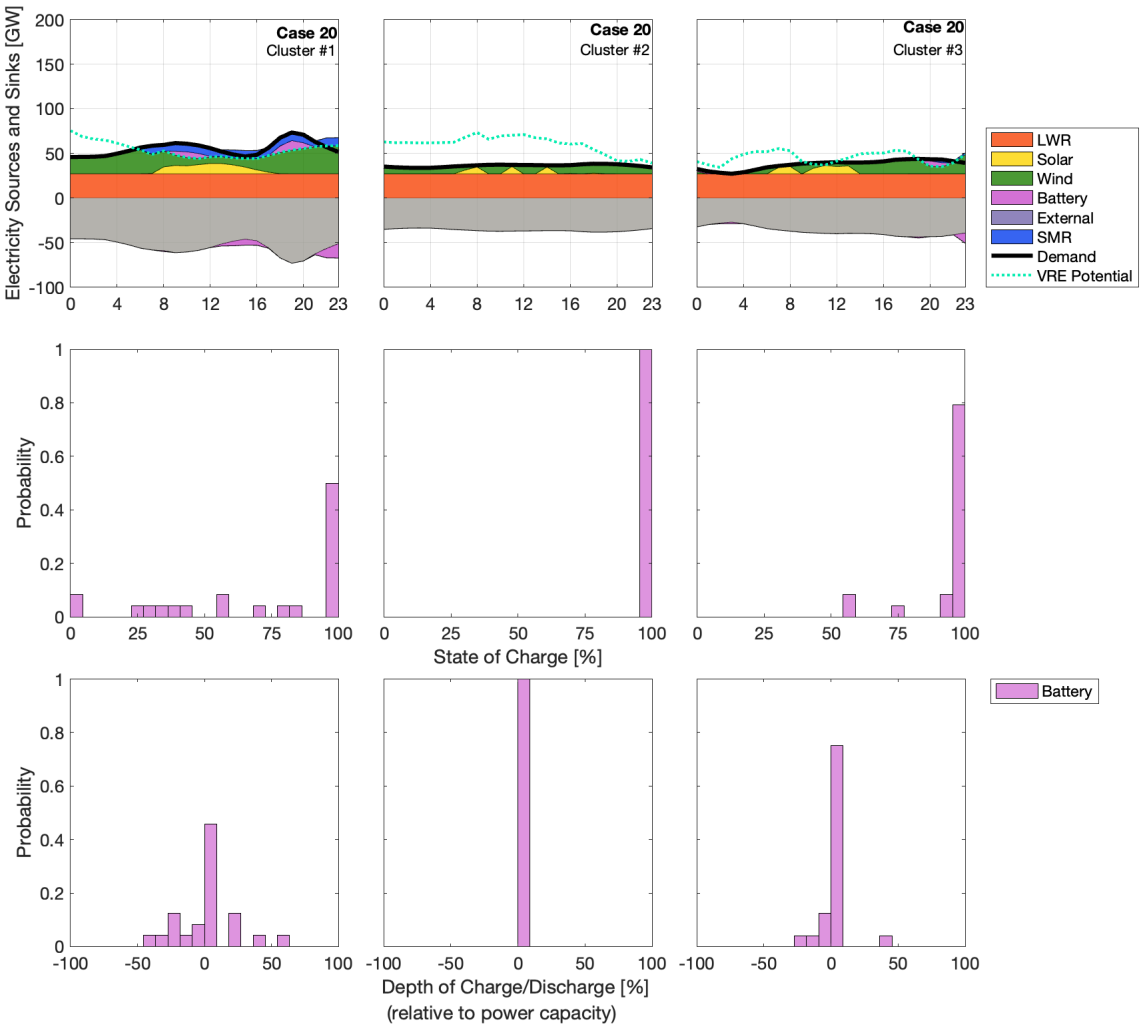

Figure A-20. Hourly dispatch of optimal generation mix with 1-day temporal extent, as obtained through cost-minimization, showcasing the least-cost portfolio. This figure shows 1 day of dispatch for each of three clusters, along with the corresponding hourly charge (+) and discharge (-) (relative to their own respective power capacities) for battery storage.

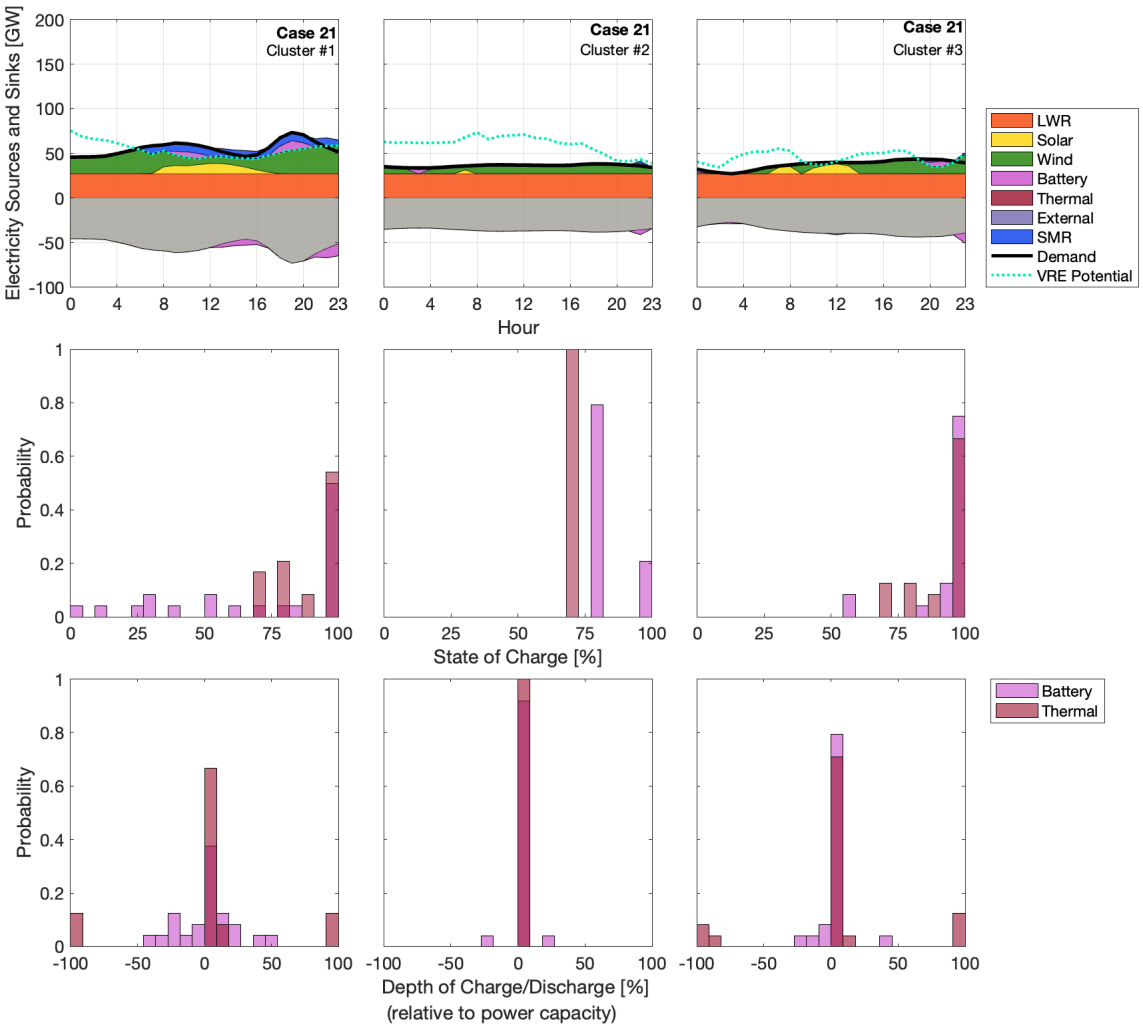

Figure A-21. Hourly dispatch of optimal generation mix with 1-day temporal extent, as obtained through cost-minimization, showcasing the least-cost portfolio. This figure shows 1 day of dispatch for each of three clusters, along with the corresponding hourly charge (+) and discharge (-) (relative to their own respective power capacities) for battery and thermal storage.

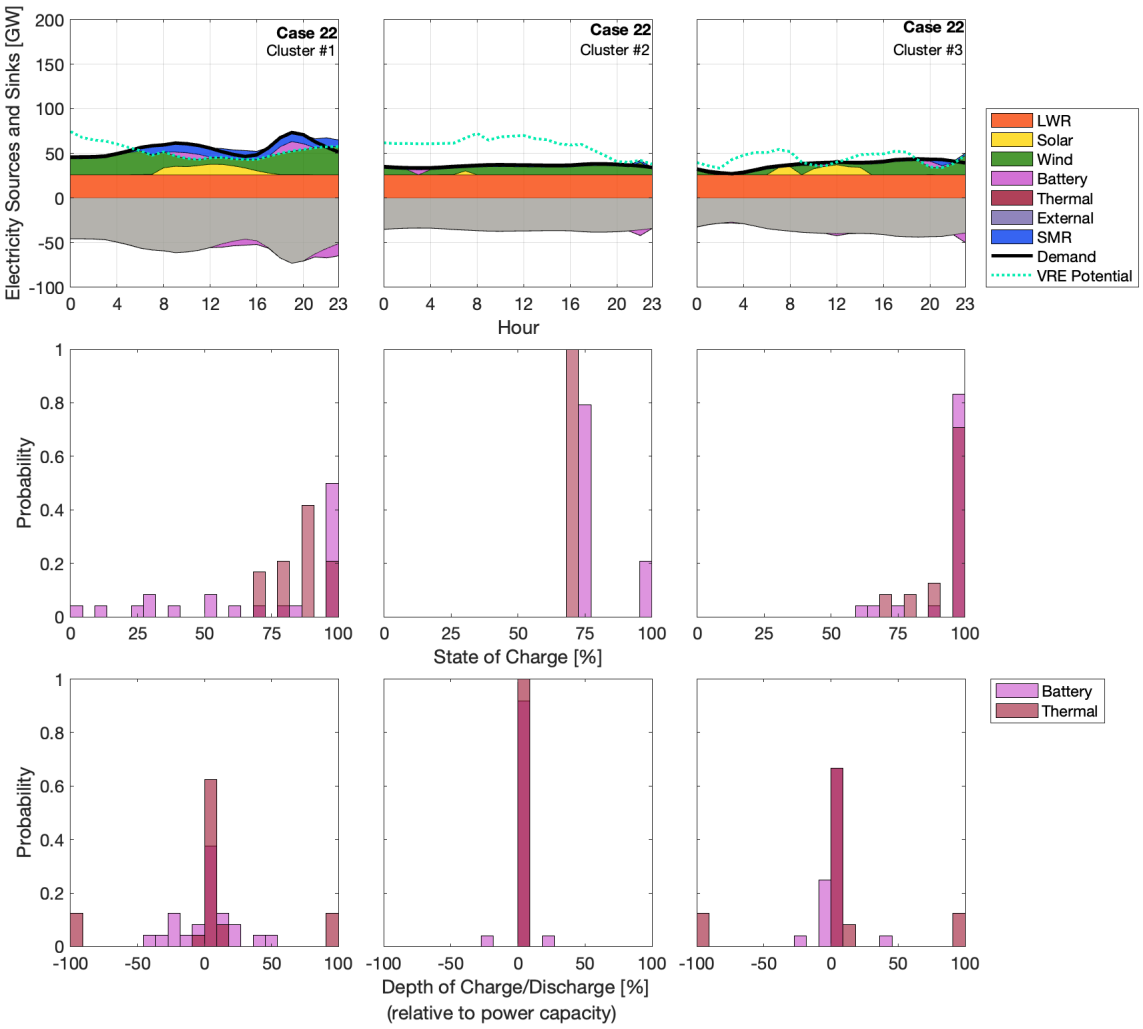

Figure A-22. Hourly dispatch of optimal generation mix with 1-day temporal extent, as obtained through cost-minimization, showcasing the least-cost portfolio. This figure shows 1 day of dispatch for each of three clusters, along with the corresponding hourly charge (+) and discharge (-) (relative to their own respective power capacities) for battery and thermal storage.

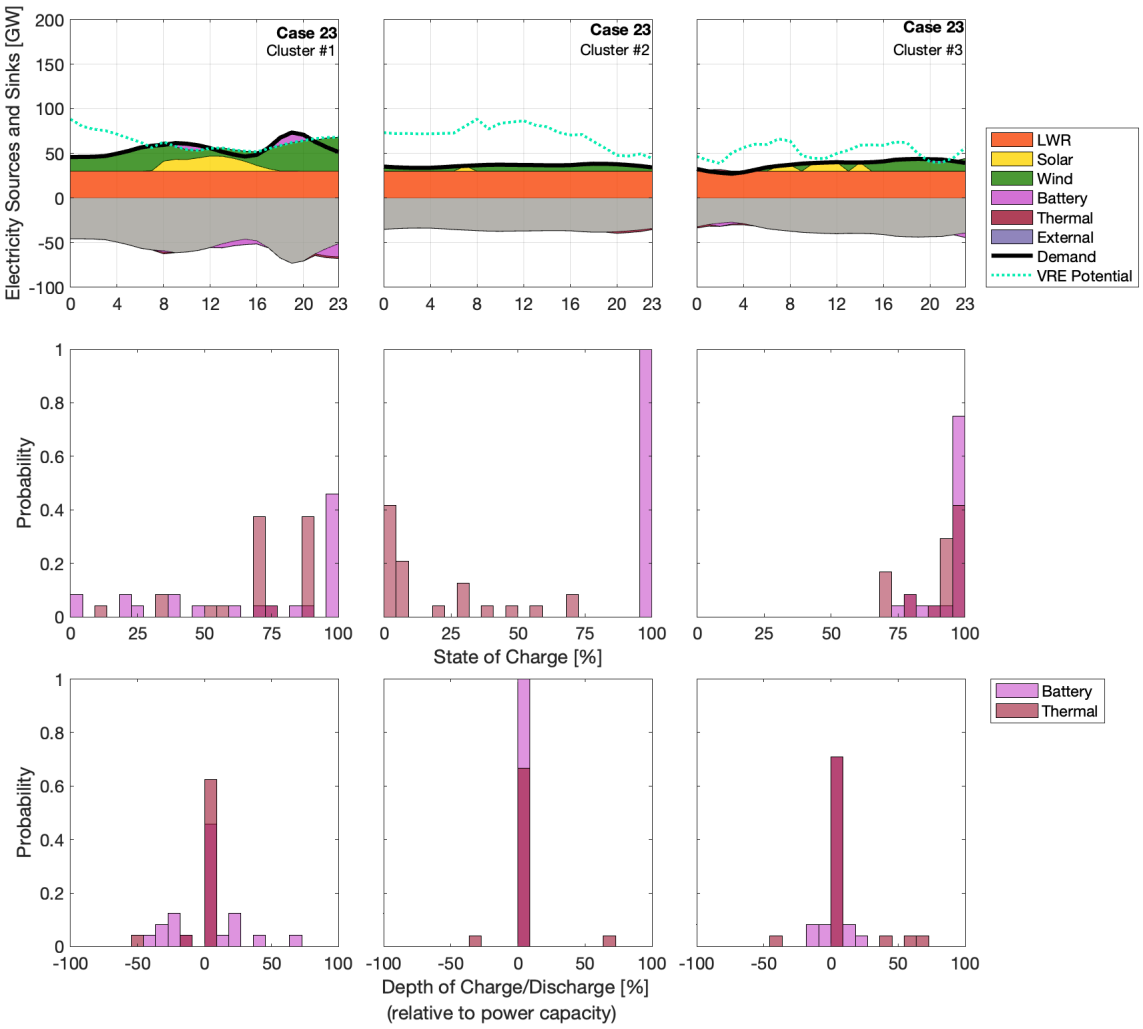

Figure A-23. Hourly dispatch of optimal generation mix with 1-day temporal extent, as obtained through cost-minimization, showcasing the least-cost portfolio. This figure shows 1 day of dispatch for each of three clusters, along with the corresponding hourly charge (+) and discharge (-) (relative to their own respective power capacities) for battery and thermal storage.

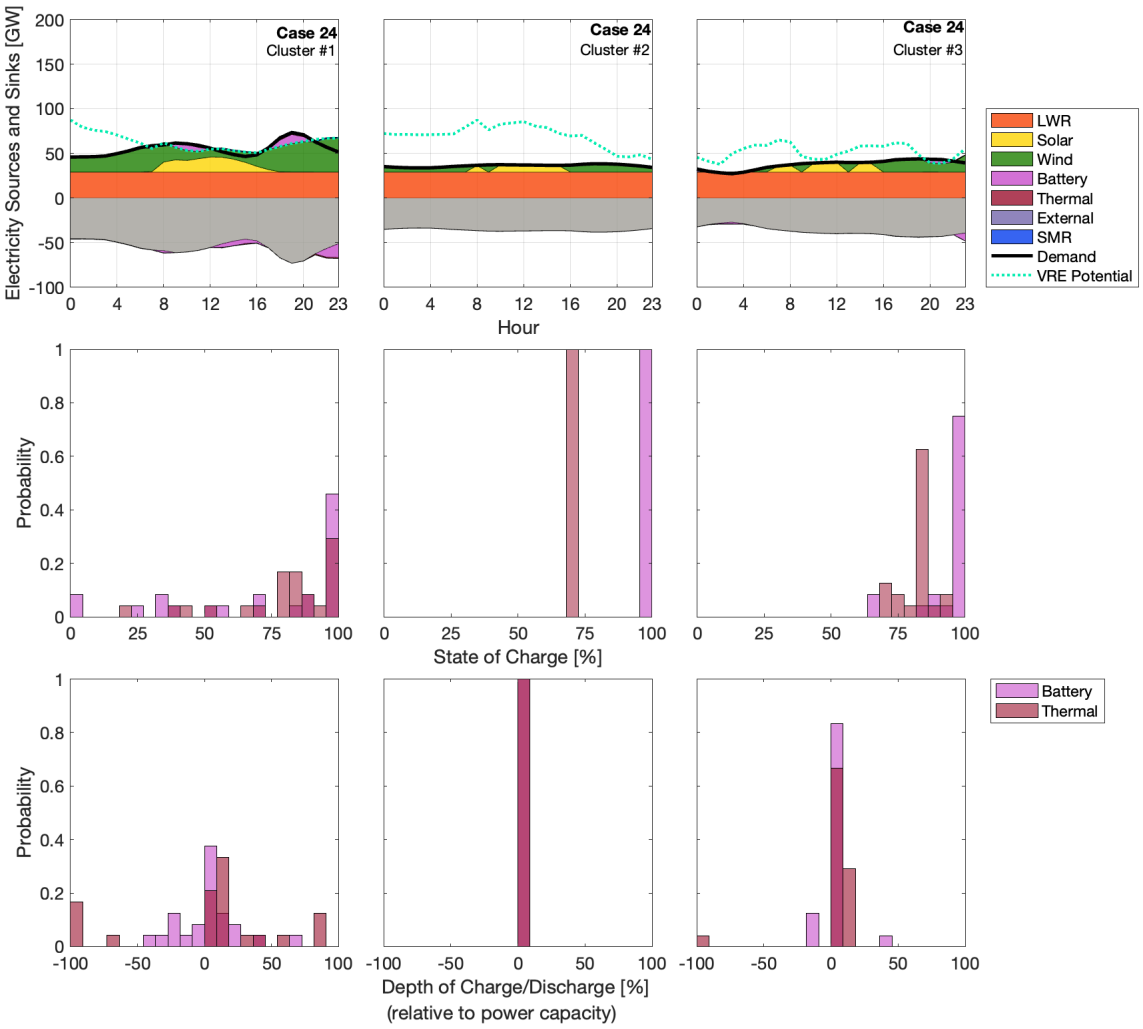

Figure A-24. Hourly dispatch of optimal generation mix with 1-day temporal extent, as obtained through cost-minimization, showcasing the least-cost portfolio. This figure shows 1 day of dispatch for each of three clusters, along with the corresponding hourly charge (+) and discharge (-) (relative to their own respective power capacities) for battery and thermal storage.